University of Bergen
Department of Mathematics

Wave response to an arbitrary motion of a load on an ice plate

Author: Kristoffer Johnsen
Supervisors: Henrik Kalisch (Professor of Applied Mathematics, University of Bergen)

UNIVERSITETET I BERGEN
Det matematisk-naturvitenskapelige fakultet

June, 2022

Abstract

This master thesis aims to explore the linear 2 dimensional ice wave model proposed by [5], where they presented a solution for loads moving in a straight path. In this thesis the solution is extended to also describe arbitrary pressure distributions with their time evolution. A solution capable of covering everything from a plane lifting off to a car doing doughnuts.

This solution is then used to explore wave patterns of different paths. Thereby finding possible dangerous scenarios involving other than linear paths, possibly leading to ice failure. To achieve this goal we are going to use the same pseudo-Fourier spectral method, as in the paper [5], using the FFT (Fast Fourier method) in space, and then the Laplace transform to compute the time evolution. But by modifying the Laplace expression a more general solution can be found. Though this solution involves an integral, it is better than a convolution for reasons that will be made apparent later.

As a second part, presented in chapter 5, we are going to employ a different transform method in space the Hankel transform. This is also referred to as the Fourier-Bessel transform, a method that lends itself well to the circular path problem. We are going to keep the Laplace transform in time. The Hankel transform as the Fourier transform has a "fast transform method" making the computations fairly cheep but most importantly it removes the time domains cost factor in the computation.

Acknowledgements

First and foremost, I would like to thank my supervisor Prof. Henrik Kalisch, for both great and challenging assignment. And for all the supervision along the way.

I would also like to thank Prof. Emilian I. Părău, from the university of East Anglia for the help in the project and for co-writing the paper.

Finally, I would like to thank my parents, for among other things forcing me to do my math homework in elementary school. Hopefully this serves as a warning to other parents of what might happen if such is done.

And a thanks to Liv Merete Jacobsen, and Børge Kristoffersen for help in proofreading.

`Kristoffer Johnsen`
Wednesday 22nd June, 2022

Contents

1 Introduction **1**
1.1 Historical view 1
1.2 Outline 2

2 Fluid and solid mechanics **4**
2.1 The ice-plate water system 4
2.2 The linear dispersion relation and critical speed 10
2.3 Stress in a beam of thickness h 16

3 Solving the PDE-system **17**
3.1 The linear velocity case 20
3.2 Numerical methods 22

4 Results **25**
4.1 Circular case 27
4.2 Different distributions, the rectangular case 31
4.3 Convergence of the solution when using a delta distribution 33
4.4 Driving a car on the ice while trying to avoid an obstacle 35

5 An alternative transform method in space, The Hankel transform **37**
5.1 Transform methods 37
5.2 Hankel-transform using Quasi Fast Hankel Transform (FHT) 41

6 Summary and further work **44**

Bibliography **46**

A Code used in the experiments **57**

List of Figures

2.1 Ice water system illustrative figure 5
2.2 Dispersion relation "Lake Saroma" 12
2.3 Wave patterns for different speeds "Lake Saroma" 13
2.4 Non-Dimensional Critical speed 15

3.1 Strain measurement along central line compared to alternative model . . 23

4.1 Comparing the maximum ice depression of the DKP model to the Takizawa filed report data 26
4.2 $\varepsilon_{max} \times 10^{-4}$ as a function of velocity, after $t = 100s$ 27
4.3 Circular path contour-plot with linear velocity path as initial condition . 28
4.4 3-D plots of circular path 28
4.5 3-D plot of circular path 28
4.6 Plotting of stress circular path vs linear path 29
4.7 plot of amplitude along the x axis for different times t 30
4.8 Rectangular (40m x 4m) shaped pressure distribution travelling over the ice, short side towards the direction of travel 31
4.9 Rectangular (4m x 40m) shaped pressure distribution travelling over the ice, long side towards the direction of travel 32
4.10 Shows the central line of η of the plots for the different number of grid points m 33
4.11 Shows the central line of the plots for the different values of m 34
4.12 Comparison of stress for different paths 36

5.1 Hankel transform contour-plot close up 41
5.2 Hankel Transform 2 42
5.3 Comparison Hankel transform and Fourier transform 43

List of Tables

2.1 Parameters describing the ice 5
2.2 Table showing the values from different field studies 14

Listings

A.1 Computing Critical Speed 57
A.2 Computing the common operators for use in the different cases 57
A.3 Example circular path first version 59

Chapter 1

Introduction

1.1 Historical view

Transport across ice-covered areas has been done through the ages. A process that can be a hazardous endeavour, hence there is a great interest in having good models to minimize risks. Duress on a floating ice sheet system by planes landing or taking off, motorized vehicles or sleds is typical for areas like Canada, Russia or Alaska, especially during the winter months. So, these countries rely on mathematical models to describe the influence of moving pressure distribution for their transport sectors safety[1].

As has been done in this master thesis, the models usually consist of a water model and a separate ice sheet model. These models are then combined into a more advanced convoluted model taking into account the different forces and effects in play. Such a combined water model can be justified, similarly to how surface gravity waves are modelled [9, 16, 19, 10]. The waves induced have been explored in earlier works by [21, 20]. The ice sheet is usually, though not always, modelled as a thin plate. These thin plate equations constitute a large and rich field with many types of models and combinations of models. But usually, because the amplitude is fairly small compared to the wavelength, simpler models may be quite correct. And because simpler models usually are easier to manipulate, they are usually preferable to the more advanced ones. Because of the small-amplitude η, linear models are usually very correct, and this follows the classical works in [20, 21] also elaborated in [18]. Some strides have been made into the non-linear analysis realm [5, 11], but we will only consider the linear equations here.

1.2 Outline

In this master thesis, we will investigate the hydrodynamical laws that govern the ice water system. In particular we will analyse the extended 2D model that allows for a full planar look at the ice-water systems response to a moving load. This is done by describing the induced pressure distribution from the load to the ice sheet $P(\vec{x}, t)$ with a time evolution. As only unidirectional paths where modelled in [5] the work done here is to extend the solution to also cover more general paths and time evolutions. We will then use this solution to look at the specific example of circular paths, and paths involving both circular and linear parts. In theory, any trajectory is possible with any time evolution, but some time evolutions are more difficult to work with than others.

The thesis is partitioned in 6 chapters including this introduction chapter, and a short paper that will be submitted shortly. Chapters 2, 3, 4 and 5 will cover various topics about and related to the ice-water model. In **Chapter 2**, we will go through the concepts and framework we need to understand the model and the solution. Mainly focusing on the derivation of the partial differential equation (PDE) system from a slightly simpler and more direct approach. Using the well known idealized fluid equations coupled with the thin beam equation and the Dirichlet-Neuman operator. Then we need an introduction to the dispersion relation, and how it is related to the important concept of critical speed, denoted by u_c.

Chapter 3 will be dedicated to solving the main Partial Differential Equation (PDE) system shown in chapter 2. First deriving the solution for the most general form. Then by making specifications to the pressure distributions, we can solve it for any path. Finally looking at the specific linear velocity case showing that this solution is the same as presented in [5].

Chapter 4 will be dedicated to testing the solution and exploring the wave response to curved load paths. Starting with the comparison to the real world data presented in[20] with the output given by the solution presented in chapter 3. Then we will show how our model handles different paths and pressure distributions. And we will also take a look at the model's predicted stress, for different paths.

In **Chapter 5** we are going to look at an alternative way of solving the PDE-system using the Hankel transform/Bessel expansion. This will be done to remove the time integration for a more computationally efficient solution for the circular case. A formal

justification will be presented. Here we used the FHT (Fast Hankel Transform) to numerically compute the solution in space. And to the best of our knowledge, this is the first time where the FHT has been used to approximate a non-radially symmetrical problem. We observed some discrepancies in the numerical results of the Hankel Transform method compared to the numerical results in Chapter 3, however it still gives useful information.

The short paper in the appendix is based on the model and solution presented in chapter 3 and 4. Chapter 3 4 and 5 except the solution for the linear velocity in chapter 3, constitutes the new results.

Chapter 2

Fluid and solid mechanics

In this part, we will start by describing the continuum-mechanical models and laws needed to describe the ice floe-water system. The simplifications and methods used to get to the PDE-system are as given in [5]. The approach though similar will follow a simpler but more direct path to the linear PDE system, but will do so for the full 3-dimensional system of equations. After the linearised PDE is presented the focus will be on the important concepts of the dispersion relation. Following this up with how the dispersion relation is related to the critical speed and wavelength. Next, a dimensional analysis is used to describe how the system reacts to different changes of the system parameters. The section will end with a short description of how to model strain in an ice sheet from the known amplitude $\eta(x, y)$ using the thin beam approximation.

2.1 The ice-plate water system

The first thing to do is to get an overview of which parameters and physical laws the ice-plate water system consists of. How they are needed to describe the system, which simplifications are needed, and how this all ties together. Figure 2.1 gives an overview of the different parameters conventions needed.

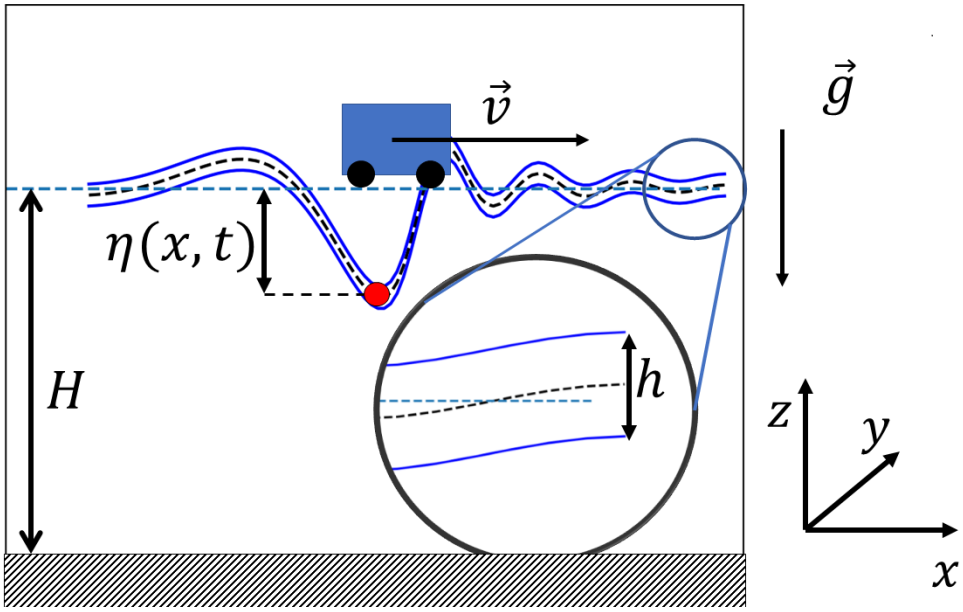

Figure 2.1: Ice water system illustrative figure

H is the water depth, $\eta(x,(y),t)$ is the amplitude and h is the ice thickens. The coordinate system convention used is z in the vertical direction and x, eventually also y, in the horizontal direction(s).

H is the water depth to the neutral position of the ice, h denotes the thickness of the ice sheet; ρ and ρ_I are the density of the water and the ice respectively. In addition we also need g the gravitational constant as well as the orientation upwards making $\vec{g} = -[0, 0, g]$. The following constants and parameters are also needed to get a complete description but does not have a physical measurement that is easy to picture:

σ (0.3)	Poissons ratio	ρ_I	Ice density
E	Elastic modulus	ρ	Water density
D	Flexural rigidity	ϕ	Velocity potential in Water
L	Characteristic length	Φ	Surface velocity potential

Table 2.1: Parameters describing the ice

These variables are not all independent. On the left hand side of table 2.1 we have some useful relationships for anyone trying to replicate the experiments or calculations done later on.

$$L = \left[\frac{Eh^3}{12\rho g(1-\sigma)}\right]^{1/4}, \; D = \frac{Eh^3}{12(1-\sigma^2)} \tag{2.1}$$

These are the main conventions and parameters used. We are now ready for the first part of the ice water system, the fluid part. To this part we are going to use the simplest conservation law conservation of mass, expressed in terms of the continuity equation, with the velocity field u:

$$\frac{\partial \rho}{\partial t} + \nabla \cdot (\rho u) = \frac{\partial \rho}{\partial t} + \rho \nabla(u) + u \cdot \nabla \rho = 0 \tag{2.2}$$

2.2 should here be considered the full 3D version and relates the density/mas flux with the momentum. Now we are going to make the first simplification, that is to assume the fluid to be incompressible. In terms of equations 2.2 this is given by the material derivative $\frac{D\rho}{Dt} = \frac{\partial \rho}{\partial t} + u \cdot \nabla \rho = 0$. Leaving us with only the Laplace equation $\rho \nabla \cdot u = 0$. Now as ρ cannot always be zero, unless we are in a vacuum, we are left with $\nabla \cdot u = 0$. Now through the Cauchy-equation in complex variable this implies that, as long as the domain is simply connected, there exists a unique velocity potential $\phi(x, y, z, t)$ such that the velocity of the water $u(x, t)$ can be written as the gradient of a velocity potential ϕ, $\nabla \phi = u$. So we are now left with discussing solutions in the water of the form:

$$\nabla \cdot u = \triangle \phi = 0 \;\; (x, y, z) \in \mathbb{R}^2 \times (-H, \eta) \tag{2.3}$$

Lastly for the water part we need the conservation of momentum equation, which is the Navier-stokes equation. But as we already have an equation 2.3 describing the flow, the Navier-stokes equation is reduced to the Bernoulli's equation (2.4). We still need it though as we currently have no way of describing external pressure imposed on the fluid, and pressure/force is the way of describing the relationship between the ice and fluid.Thus leaving us with the equation:

$$\frac{\partial \phi}{\partial t} + \frac{1}{2}u^2 + \frac{p}{\rho} + gz = c \tag{2.4}$$

Next we need to discuss the boundary conditions that is imposed on the fluid. For the sea bed the choice is the no flow through the boundary condition, represented by:

$$\frac{\partial \phi}{\partial z} = 0 \mid_{z=-H} \tag{2.5}$$

The next we need is the kinematic conditions at the surface boundary condition, expressing that the water is moving at the same velocity at the boundary as the ice, meaning that we have no flow through, but also that there is no creation of separation between

the fluid and the ice.

$$(\vec{n} \cdot \vec{u})_{z=\eta(x,t)} = (\vec{n} \cdot \vec{u}_s) = \eta_t + \phi_x \eta_x + \phi_y \eta_y - \phi_z = 0 \mid_{z=\eta(x,t)} \tag{2.6}$$

Then we need a suitable beam equation and the one used here is (2.7), and since η is the only displacement of the beam it only makes sense to also use that variable here as well. The b coefficient is the damping, we define this by the non dimensional damping as used in [20],[18]. The non-dimensional damping coefficient is $B = 2\sqrt{\rho g \rho_I h}$. The one used however is the dimensional damping coefficient. The beam equation uses the displacement variable and for the thin plate that would be the displacement in the z direction. But as we already have a variable for that η we are going to use that here.

$$D\triangle^2\eta - \frac{\rho_I h^3}{12}\partial_t^2\triangle\eta + \rho_I h\partial_t^2\eta + b\partial_t\eta + \rho_I g\eta + P - p = 0 \tag{2.7}$$

In this equation P is the upper pressure induced by the load, and the small p is the pressure from the water underneath. Using the Bernoulli equation with $c = \frac{\rho_I g h}{\rho}$ to describe the water ice pressure. We get the following equation $\frac{p}{\rho} = \frac{\rho_I g h}{\rho} - g\eta - \phi_t - 0.5|\nabla\phi|^2$. Putting all of this into the beam equation (2.7) and dividing by the constant water density ρ in the beam equation as well yields the following result.

$$\frac{D}{\rho}\triangle^2\eta - \frac{\rho_I h^3}{\rho 12}\partial_t^2\triangle\eta + \frac{\rho_I h}{\rho}\partial_t^2\eta + \frac{b}{\rho}\partial_t\eta + \frac{\rho_I g h}{\rho} + \frac{P}{\rho} + \frac{1}{2}|\nabla\phi|^2 + g\eta - \frac{\rho_I g h}{\rho} = 0 \tag{2.8}$$

Simplifying expression (2.8) and including the kinematic boundary we get the following set of partial differential equations.

$$\eta_t + \phi_x\eta_x + \phi_y\eta_y - \phi_z = 0\big|_{z=\eta} \tag{2.9}$$

$$\frac{D}{\rho}\triangle^2\eta - \frac{\rho_I h^3}{\rho 12}\partial_t^2\triangle\eta + \frac{\rho_I h}{\rho}\partial_t^2\eta + \frac{b}{\rho}\partial_t\eta + \frac{\rho_I g}{\rho}\eta + \frac{P}{\rho} - g\eta + \phi_t + \frac{1}{2}|\nabla\phi|^2 = 0\Big|_{z=\eta} \tag{2.10}$$

Next we are going to introduce the the surface velocity potential, i.e the velocity potential along the ice water interface $\Phi(x, y, t) = \phi(x, y, \eta(x, y, t), t)$. And we are going to make use of the Dirichlet-Neumann operator G. From [4, 13] we know that this operator can be defined in such a way that it satisfy the following relationship:

$$G(\eta)\Phi = \partial_z\phi - \partial_x\eta\partial_x\phi - \partial_y\eta\partial_y\phi\big|_{z=\eta} \tag{2.11}$$

Now this immediately reduces the kinematic boundary condition to:

$$\eta_t = G\Phi \tag{2.12}$$

Next we are going to look at the other governing equation (2.10). From this we have three things we need to simplify $\partial_t^2\eta$, $\partial_t\eta$ and $\partial_t\phi + 0.5|\nabla\phi|^2$. First we have from the new kinematic boundary condition (2.12) which makes $\eta_t = G\Phi$. Next we have $\partial_t^2\eta = \partial_t(G\Phi)$ and we have through the definition of the surface velocity potential $\Phi_t = \phi_t + \eta_t\phi_z \implies \phi_t = \Phi_t - \eta_t\phi_z$. For the next part we need the gradient of the velocity potential written in our new variable Φ and η. For this we need the surface velocity at the boundary togheter with the definition of the Diriclet-Neuman operator 2.11.

$$u = \Phi_x = \phi_x + \phi_z\eta_x \tag{2.13}$$

$$v = \Phi_y = \phi_y + \phi_z\eta_y \tag{2.14}$$

Written in matrix form equation (2.13),(2.14),2.11 becomes:

$$\begin{bmatrix} -\eta_x & -\eta_y & 1 \\ 1 & 0 & \eta_x \\ 0 & 1 & \eta_y \end{bmatrix} \begin{bmatrix} \phi_x \\ \phi_y \\ \phi_z \end{bmatrix} = \begin{bmatrix} G\Phi \\ \Phi_x \\ \Phi_y \end{bmatrix} \tag{2.15}$$

Where the gradient in 2.15 is written out on component form. To get the gradient of the velocity potential in the new variables we need the inverse.Inverting the matrix was not simple but in the end it can be reduced to:

$$\frac{1}{\eta_x^2 + \eta_y^2 + 1} \begin{bmatrix} -\eta_x & \eta_y^2 + 1 & -\eta_x\eta_y \\ -\eta_y & -\eta_y\eta_x & \eta_x^2 + 1 \\ 1 & \eta_x & \eta_y \end{bmatrix} \begin{bmatrix} G\Phi \\ \Phi_x \\ \Phi_y \end{bmatrix} \tag{2.16}$$

$$= \frac{1}{\eta_x^2 + \eta_y^2 + 1} \begin{bmatrix} -G\Phi\eta_x + \left(\eta_y^2 + 1\right)\Phi_x + -\eta_x\eta_y\Phi_y \\ -\eta_y G\Phi - \eta_x\eta_y\Phi_x + \left(\eta_x^2 + 1\right)\Phi_y \\ G\Phi + \eta_x\Phi_x + \eta_y\Phi_y \end{bmatrix} = \begin{bmatrix} \phi_x \\ \phi_y \\ \phi_z \end{bmatrix} \tag{2.17}$$

Now $|\nabla\phi|^2$ will in the end only consist of non-linear parts in Φ and η thus when we linearise this will all be removed from the equation. We can see this from the fact that there are no parts of (2.17) that does not contain a Φ, η or any of their derivatives. But for completeness we can clean up $0.5|\nabla\phi|^2$ with the following notation $|\eta| = \sqrt{\eta_x^2 + \eta_y^2 + 1}$ as:

$$\frac{1}{2}|\nabla\phi|^2 = \frac{1}{2|\eta|^4}\left[\Phi_x^2\left(|\eta|^2(\eta_y^2+1)\right)+\Phi_y^2\left(|\eta|^2(\eta_x^2+1)\right)+(G\Phi)^2\left(|\eta|^2\right)+\Phi_x\Phi_y\left(-2\eta_x\eta_y|\eta|^2\right)\right]$$

As there are no problems with $|\eta|$ going to zero, and since all of the terms only have $|\eta|$ to the power of two we are safe to assume their all non-linear. Then we need to compute ϕ_t part, if we use the ϕ_z part form (2.17) we get:

$$\Phi_t = \phi_t + \phi_z\eta_t = \phi_t + G\Phi \implies \phi_t = \Phi_t - \phi_z G\Phi = \Phi_t - \frac{(G\Phi)^2+\eta_x\Phi_x+\eta_y\Phi_y}{\eta_x^2+\eta_y^2+1} \quad (2.18)$$

Of which only the first part Φ_t is linear. Then over to the last term that we need to simplify $\partial_t(G\Phi)$

Here we need the series expansion of the Diriclet-Neuman operator here acting on Φ:

$$G(\eta)\Phi = \sum_i G_i\Phi \quad (2.19)$$

Using the notation common to this operator $D = (i\partial_x, i\partial_y)$, $|D| = \sqrt{-\partial_x^2-\partial_x^2}$ the first three terms are [4, 13].

$$G_0(\eta) = |D|\tanh(H|D|)\ ,\ G_1(\eta) = -\partial_x\eta\partial_x - \partial_y\eta\partial_y - G_0\eta G_0\ ,$$
$$G_2 = G_2(\eta) = -0.5(|D|^2\eta^2 G_0 + G_0\eta^2|D|^2 - 2G_0\eta G_0\eta G_0$$

As we can see all of them except the G_0 operator is dependant on η meaning if applied to a Φ will result in a non-linear term, this will also be used later. But for the $\partial_t(G\Phi)$ this means that $\partial_t(G\Phi) = \sum_i \partial_t G_i(\eta)\Phi = \sum_i G_i\partial_t\Phi + \partial_\eta G(\eta)\eta_t$ Now unless G_i is independent of η this will not be linear, and the only one this is valid for is G_0. This therefore reduces $\partial_t(G\Phi) \approx G_0\Phi_t$. Then putting all of this into (2.10) and making sure to approximate $G \approx G_0$ we are left with:

$$g\chi\triangle^2\eta - \frac{\rho_I h^3}{\rho 12}\triangle G_0\Phi_t + \frac{\rho_I h}{\rho}G_0\Phi_t + bG_0\Phi + P + g\eta + \Phi_t = 0 \quad (2.20)$$

Then rearranging the terms into Φ, Φ_t, η in (2.20):

$$-g(\chi\triangle^2+1)\eta - \frac{b}{\rho}G_0\Phi - \frac{P}{\rho} = \left(1+\frac{h\rho_I}{\rho}(1-\frac{h^2\triangle}{12})G_0\right)\Phi_t \quad (2.21)$$

Then defining the operator $K = 1+\frac{h\rho_I}{\rho}(1-\frac{h^2\triangle}{12})G_0$ with the Fourier equivalent operator $k(\xi) = 1+\frac{h\rho_I}{\rho}(1+\frac{h^2|\xi|^2}{12})G_0$ which is invertible due to the fact that $k(\xi) \geq 1$ therefore we

can do a final rewriting of (2.20) together with the kinematic boundary condition.

$$\eta_t = G_0\Phi \tag{2.22}$$

$$\Phi_t = -g\frac{(\chi\triangle^2+1)}{K}\eta - \frac{bG_0}{\rho K}\Phi - \frac{P}{\rho K} \tag{2.23}$$

If we substitute w for $\frac{P}{\rho K}$ we get our main PDE system. To make this more accurate one could save more terms in the Diriclet-Neumann operator like quadratic terms or higher.

2.2 The linear dispersion relation and critical speed

Here we are going to replicate the procedure presented [20]. First, we are going to present the linear system usually used to compute the dispersion relation and use this to define the critical speed. If we take the same system, but exchange the kinematic boundary condition for the more simpler linearised Bernoulli equation [18] we get:

$$p = -\rho g\eta - \rho\frac{\partial\phi}{\partial t}\bigg|_{z=\eta} \tag{2.24}$$

The Laplace equation 2.3 for u and the non dampened beam equation without the rotary term and with only a pressure term p acting from below on the ice from the water:

$$D\nabla^4\eta + \rho_I h\frac{\partial^2\eta}{\partial t^2} = p \tag{2.25}$$

The dispersion relation, is a relationship between wave lengths and wave speed, for travelling waves of the form

$$\eta(x,t) = \eta_0\cos(k(x-ct)) \tag{2.26}$$

This then has the potential function of the form:

$$\phi = A\cosh(k[z+H])\sin(k(x-ct)) \tag{2.27}$$

The ice should always be in contact with the water:

$$\frac{\partial\phi}{\partial z} = \frac{\partial\eta}{\partial t}\bigg|_{z=\eta} \tag{2.28}$$

Using ϕ from the equation (2.27) together with the equation for η (2.26) into equation (2.27) yields us $\frac{A}{k}\cosh(k[z+H])\sin(k(x-ct)) = \frac{\eta_0}{kc}\sin(k(x-ct))$ Assume that $\eta << H$

we get the relationship:

$$A = \frac{\eta_0 c}{\sinh(kH)} \tag{2.29}$$

The last step is to putt all of this back into the non-dampend beam equation (2.25) with the linearised Bernoulli equation (2.24) for the pressure p.

$$\begin{aligned} &\left(k^4 D + (kc)^2 \rho_i h\right) \eta_0 \cos(k(x-ct)) \\ &= -\rho \eta_0 g - \rho_w \frac{\eta_0 c^2 k}{\sinh(kH)} \cosh(k(z+H)) \cos(k(x-ct)) \end{aligned}$$

Giving us the following equation:

$$c^2 = \frac{Dk^3/\rho + g/k}{\rho_I hk/\rho_w + 1/\tanh(kH)} \approx \frac{Dk^3/\rho + g/k}{1/\tanh(kH)} \, , \lambda >> h \implies \rho_I hk/\rho_w \to 0 \tag{2.30}$$

And we are left with the dispersion relation:

$$c^2 = \frac{g}{k}\left(1 + Lk^4\right)\tanh(kH) = \frac{g}{\frac{2\pi}{\lambda}}\left(1 + L\frac{2\pi}{\lambda}^4\right)\tanh(\frac{2\pi}{\lambda}H) \tag{2.31}$$

If we now take the lake Samora case, with data from [20] here $L = 2.20$ and $H = 6.8$, more numbers are presented underneath, we can plot the wave speed c of different values of λ and we get a dispersion curve with a characteristic minimum:

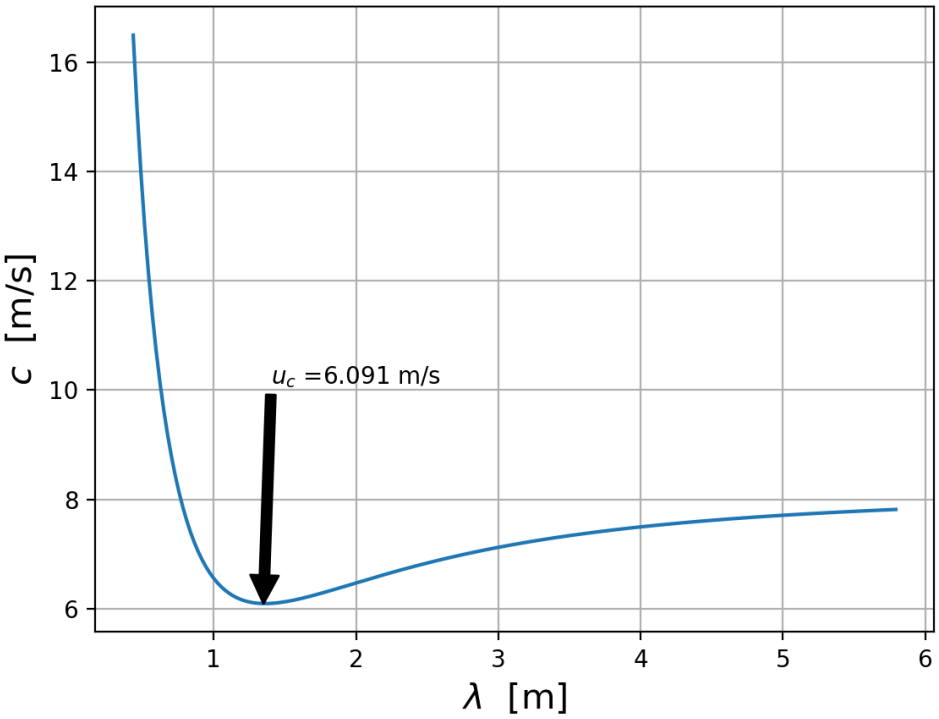

Figure 2.2: Dispersion relation "Lake Saroma"

Shows the wave speed c of the wave length λ. Numbers for this lake can be found in table 2.2.

The first thing we need to note is that as the wave length λ goes to zero the wave speed goes to ∞. The next thing is the area between $6m/s < c < 8m/s$ where 2 wavelengths have the same speed, culminating in the u_c here equal to $6.091m/s$. This c is a global minimum and is generally referred to as the critical speed u_c.

If we view it from the perspective of the model we get different results for the different velocities. It is also well known that the minimum of the load speed does coincide with $c_{min} = u_c$ [20].Next we have plotted 4 cases for different parts of the speed regime.

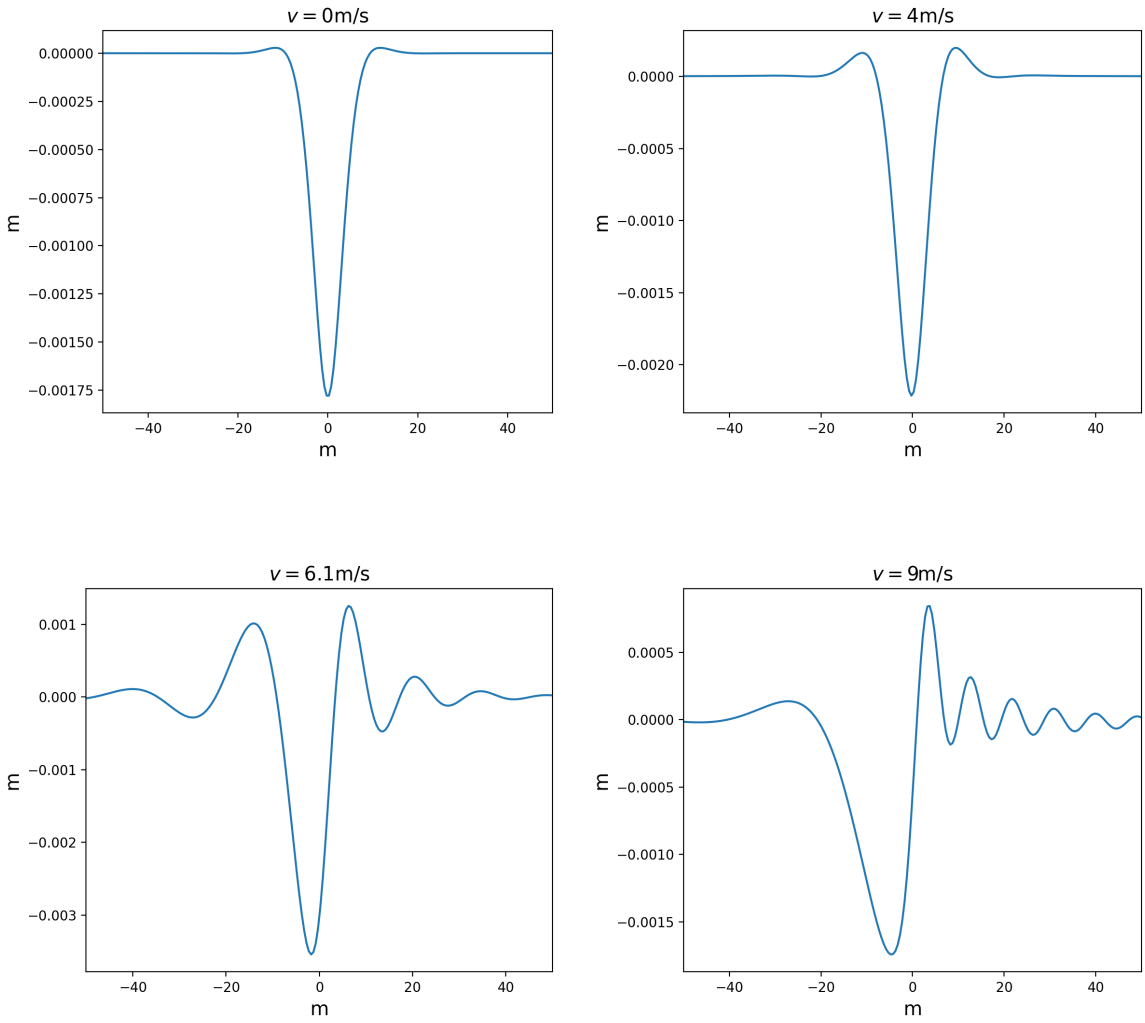

Figure 2.3: Wave patterns for different speeds "Lake Saroma"

For illustrative purpose Lake Samora was used as an example of what happens when you are in the different parts of the speed regime. $u_c = 6.09m/s$ and the different plots shows the cases when $v = 4m/s, 0m/s << u_c$, $v = 6.1m/s \approx u_c$ and $v = 9m/s >> u_c$ relatively speaking. We can see that when $v = 4m/s$ the amplitude profile is almost the same as $v = 0m/s$. When v reaches $6.1m/s$ we see that a full wave profile has been created, both trailing and front waves. In the last picture when $v = 9m/s$ the front waves remains, but the trailing waves are almost gone. In addition the amplitude is significantly reduced from when $v = 6.1m/s$. This corresponds to the real world where the maximum amplitude is reached when $v \approx u_c$[20].

To analyse the notion of critical speed further we need the dimensional analysis of the dispersion relation (2.31). Defining the non-dimensional speed and wavelength as:

$$U = \frac{u}{\sqrt{gL}} \ , \ X = \frac{\lambda}{2\pi L}$$

Denoting them by capital letters U and X, where u is the wave velocity, λ is the wave

length, and L is the characteristic length as discussed previously. Substituting the inverses into (2.31) we get:

$$U^2 = (X + 1/X^3) \tanh\left(\frac{H}{L}\frac{1}{X}\right) \tag{2.32}$$

To evaluate the critical one needs to find the minimum of this relation with respect to the wave speed. This is done by finding $\frac{dU}{dX} = 0$. This gives us the following equation for X_c

$$X_c = \left[\frac{3 + (2\frac{H}{L}\frac{1}{X_c}/\sinh(2\frac{H}{L}\frac{1}{X_c})}{1 - (2\frac{H}{L}\frac{1}{X_c}/\sinh(2\frac{H}{L}\frac{1}{X_c})}\right]^{\frac{1}{4}} \tag{2.33}$$

This equation is most usually computed numerically. Then to get the critical speed we only need insert the value X_c for X in(2.32). And then take the square root:

$$U_c = \sqrt{X_c + 1/X_c^3) \tanh\left(\frac{H}{L}\frac{1}{X_c}\right)} \tag{2.34}$$

We can now start looking at a number of lakes with different values for L and H as well as many points in between:

locations/paramters		Lake Saroma	Cold Lake	Mille Lacs	McMurdo Sound
Ice thickness	h	0.17-0.2	0.59	0.61	2.5
Elastic modulus	E	5.1e+8	4.9e+9	9e+9	5e+9
Flexural rigidity	D	2.35e+5	9.4e+7	1.91e+8	7.32e+9
Ice thiknes	h	1.70e-01	5.90e-01	6.10e-01	2.50
Water density	ρ	1.03e+03	1.02e+03	1.02e+03	1.02e+03
Water depth	H	6.8	4.3	3.26	350
Characteristic Length	L	2.20	9.84	1.18e+01	2.92e+01
	H/L	3.09	4.37e-01	2.77e-01	1.20e+01

Table 2.2: Table showing the values from different field studies

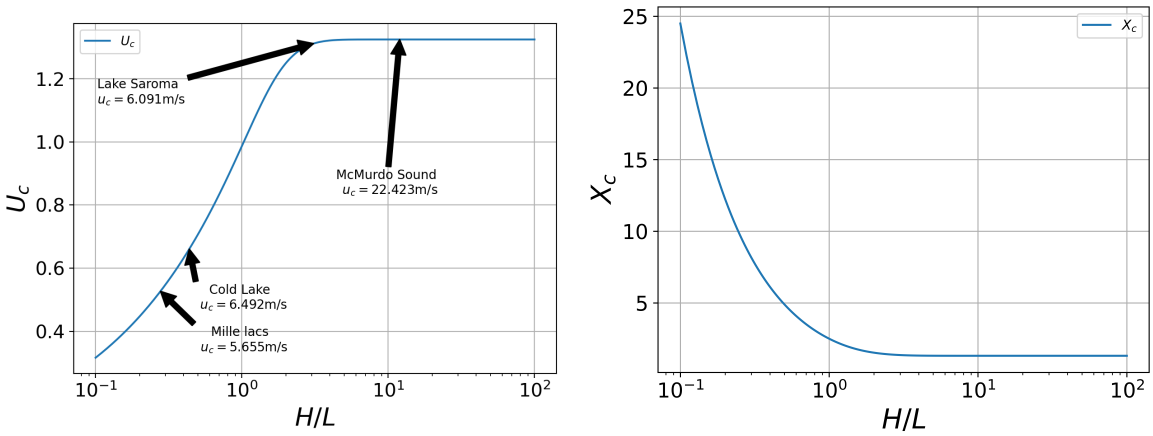

Figure 2.4: Non-Dimensional Critical speed

The actual critical speed is $u_c = U_c\sqrt{gL}$, and $x_c = \lambda/(2\pi L)$ There are as well some examples with the critical speed added on

2.4 shows the relationship between the non-dimensional critical speed U_c and critical wavelength X_c to the non-dimensional number H/L. First, we need to note that the plots are logarithmically in H/L. Next we can see that $U_c$goes very slowly towards zero. As L is of the order 1 to 10 H has to be smaller than 1/10 to 1/100 meters for the non-dimensional critical speed to be less than $0.3U_c$. The only other way of letting u_c the non dimensional speed go to zero is to let L go to zero implying that either E or h has to go to zero. As the Elastic modulus E cannot go to zero as it is defined from the type of ice it is that only leaves us with the thickens h and if that goes to zero then we have no ice. This means that in general if the ice is safe to drive on we do not see critical speeds below $10km/h$. This speed is usually what professional drivers keep below in areas where the water depth is low and ice conditions are the most challenging. Further out where the water depth is greater one can usually be safe below $25km/h = 9m/s$. So in conclusion the critical speed can vary, but usually, it is possible to avoid. However, if one is in doubt $10km/h$ seems a safe upper limit [15, 8].

2.3 Stress in a beam of thickness h

Next discussing the strain in the ice, and how to measure it. The strain that will be analysed later. The model used is the linear strain model for thin plates as used in [17]. Assuming that there is no stretching of the central line through the ice, represented by the doted line in figure 2.1 we can Taylor approximate the relative displacement. In 2D the approximate displacement is given by

$$u = -z\partial_x\eta \ , \ v = -z\partial_y\eta \tag{2.35}$$

Now the strain is given as the derivative of the displacement, giving us the following approximation of the strain ϵ:

$$\epsilon \approx \nabla \begin{bmatrix} u \\ v \end{bmatrix} = \begin{bmatrix} z\partial_x\eta \\ z\partial_y\eta \end{bmatrix} = \begin{bmatrix} \partial_x^2 & \partial_x\partial_y \\ \partial_y\partial_x & \partial_y^2 \end{bmatrix} \eta \tag{2.36}$$

In the case of this thesis the only interesting part of the strain is the maximum strain which happens when $z = h$ or $-h$ and for the maximum eigenvalue yielding.

$$\varepsilon_{max} = h \cdot \lambda \tag{2.37}$$

Where lambda is the maximal eigenvalue of the Hessian matrix.

Chapter 3

Solving the PDE-system

For this section, we will solve the linearized PDE system (2.22), (2.23) , using the Fourier spectral method in space and the Laplace transform in time. We will have a look at a general solution to all paths. Then we will derive the solution for the linear path to show that we end up with the same solution as in [5]. Next we will give an introduction to how the numerical computation is done. We will then discuss some strengths/ weaknesses of the solution and a few numerical tricks that can be done to get the time evolution of more complex paths.

Starting from the linearised pde-system ((2.22),(2.23)), and substitute $w = \frac{P}{\rho K}$ we can take the Laplace transform of the system to get an algebraic system as below.

$$\begin{aligned} s\hat{\eta} - \hat{\eta_0} &= G_0\hat{\Phi} \\ s\hat{\Phi} - \hat{\Phi_0} &= -g\frac{1+\chi\triangle^2}{K}\hat{\eta} - \frac{b}{\rho}\frac{G_0}{K}\hat{\Phi} - \hat{w} \end{aligned}$$

Assuming that $\Phi_0 = \eta_0 = 0$ and substituting $\dfrac{s\hat{\eta}}{G_0}$ in for for Φ in (2.23) we are left with

$$s\frac{s\hat{\eta}}{G_0} = -g\frac{1+\chi\triangle^2}{K}\hat{\eta} - \frac{b}{\rho}\frac{G_0}{K}\frac{s\hat{\eta}}{G_0} - \hat{w} \tag{3.1}$$

Solving the algebraic equation we are left with the solution for η:

$$\hat{\eta} = \frac{-G_0\hat{w}}{s^2 + \frac{bG_0}{\rho K}s + g\dfrac{1+\chi\triangle^2}{K}G_0} = \frac{-G_0\hat{w}}{\left(s + \frac{bG_0}{\rho K2}\right)^2 - \left(\frac{bG_0}{\rho K2}\right)^2 + g\dfrac{1+\chi\triangle^2}{K}G_0} \tag{3.2}$$

The right part of the denominator is now a square and by introducing the Fourier multiplier operators:

$$R = \frac{bG_0}{2\rho K} \ , \ U = \sqrt{\frac{1 + \chi \triangle^2}{K} G_0 - R^2} \tag{3.3}$$

we are left with a solution of the from:

$$\eta = \mathcal{L}^{-1}(\hat{m}(s) \cdot \hat{w}(s)) \tag{3.4}$$

Where:

$$m = \mathcal{L}^{-1}((\frac{-G_0}{(s+R)^2 + U^2}) \tag{3.5}$$

The operators K, R, G_0 are Fourier multiplication operators. Therefore the manipulation done only makes sense in the Fourier space.The solution is not yet transformed back into the physical space but that will be done through the (FFT) Fast Fourier Transform.

From here there are at least two approaches. One is the more direct approach, to take the Laplace of w and then multiply with $\hat{m}(s)$, and then the inverse Laplace transformed. But this approach results in situations where w had no obvious Laplace Transform.

Here we are introducing an alternative approach, ignoring the fact that the w might not have an analytical solution, and instead consider the Laplace identity [6]:

$$\mathcal{L}^{-1}(\hat{m}(s) \cdot \hat{w}(s)) = \mathcal{L}^{-1}(\hat{m}(s)) * \mathcal{L}^{-1}(\hat{w}(s)) \tag{3.6}$$

Where $*$ is the convolution. We already know the $\mathcal{L}^{-1}(\hat{w}(s)) = w$, the other one $\mathcal{L}^{-1}(\hat{m}(s))$ is more tricky but can be solved [6]:

$$m(t) = \mathcal{L}^{-1}(\hat{m}(s))(t) = \frac{G_0}{2iU} \left(e^{-t(R-iU)} - e^{-t(R+iU)} \right) \tag{3.7}$$

Now we only have to solve the finite convolution integral.

$$\eta(\xi, t) = \int_0^t m(t-\tau) w(\tau) d\tau$$

For completion we are here going to present the most general solution in its fullness which is just to fill in for $m(t)$ (3.7) and use $\frac{P(\tau)}{\rho K}$ in stead of $w(\tau)$ the Fourier transformed of the pressure at time t:

$$\eta(\xi, t) = \int_0^t \frac{G_0 w_0}{2iU} \left(e^{-(t-\tau)(R-iU)} - e^{-(t-\tau)(R+iU)} \right) \frac{P(\tau)}{\rho K} d\tau \tag{3.8}$$

If we take a general distribution with a general time evolution we will need to account for a lot. By removing morphing from the possible time evolution we are left with rotation and translation that would be $P(x,t) = P_0(x - X(t))$ where $P_0 = P(x,0)$. However while translation is easy to account for in the Fourier space through the multiplication of the Fourier multiplication operator $e^{i\xi \cdot \vec{X(t)}}$, rotation is not. Therefore we are going to restrict ourselves to looking at distributions which are rotationally invariant around a point. This point will overlap with the centre of mass. If we now translate the distribution with respect to that point we don't need to account for any rotation.

Setting $w_0 = w(x,0) = \frac{P(x,0)}{\rho K}$ means that we are left with distributions with the following time evolution $\mathscr{F}(w(x,t)) = \mathscr{F}(w(x,0)) \cdot e^{iX\vec{(t)}\cdot\xi}$ where $X(t) = [x(t), y(t)]$ could be any parametrisation of the problem. Now there is no problem with having a car sliding through a turn facing the same direction, but as shown in [12] and later when we use different w_0 distribution, can have an impact on the wave patterns especially around the load. There is no problem using rotation but one usually has to rotate in the regular space and that makes the whole solution quite costly. Therefore the solution we are going to use can be written in such a way.

$$\eta = \int_0^t m(t-\tau) w_0 e^{iX\vec{(t)}\cdot\xi} d\tau \tag{3.9}$$

Inserting for $m(t)$ gives the solution that in this form enables us to take w_0 and e^{tA} part out of the integral and only look at the two exponential integral:

$$\int_0^t \frac{G_0 w_0}{2iU} \left(e^{-(t-\tau)(R-iU)} - e^{-(t-\tau)(R+iU)} \right) e^{iX\vec{(\tau)}\cdot\xi} d\tau \tag{3.10}$$

$$\frac{G_0 w_0}{2iU} \int_0^t e^{-(t-\tau)(R-iU) - iX\vec{(\tau)}\cdot\xi} - e^{-(t-\tau)(R+iU) - iX\vec{(\tau)}\cdot\xi} d\tau \tag{3.11}$$

For reasons that will be apparent later it is convenient to keep the solution as two separate integrals. However we can simplify it even further as:

$$\eta(t,\xi) = \frac{G_0 w_0}{U} \int_0^t e^{-(t-\tau)R - i\vec{X}(\tau)\cdot\xi} \sin\left[(\tau - t)U\right] d\tau \tag{3.12}$$

Φ is then from following the formula that Where $X(t) \cdot \xi$ is a general parametrisation of the path scalar-multiplied with the (ξ_1, ξ_2) Fourier 2d frequency vector. This integral can be solved analytical in some cases and in others it has to be done numerically.

Next is to look at the surface velocity potential Φ from (2.22). We can derive that $\Phi = \dfrac{\partial_t \eta}{G_0}$ starting from the η solution (3.11), taking the derivatives of the two separate integrals to get:

$$\Phi = \frac{w_0}{2iU}\frac{\partial}{\partial t}\left[\int_0^t e^{-(t-\tau)(R-iU)-iX(\vec{\tau})\cdot\xi} - e^{-(t-\tau)(R+iU)-iX(\vec{\tau})\cdot\xi} d\tau\right] \tag{3.13}$$

$$= \frac{w_0}{2iU}\left[\int_0^t \frac{e^{-(t-\tau)(R-iU)-iX(\vec{\tau})\cdot\xi}}{-R+iU} - \frac{e^{-(t-\tau)(R+iU)-iX(\vec{\tau})\cdot\xi}}{-R-iU} d\tau\right] + \tag{3.14}$$

$$\frac{w_0}{2iU}\left[\frac{e^{-iX(\vec{t})\cdot\xi}}{-R+iU-i\partial_t X(\vec{t})\cdot\xi} - \frac{e^{-iX(\vec{t})\cdot\xi}}{-R-iU-i\partial_t X(\vec{t})\cdot\xi}\right] \tag{3.15}$$

Now, from (3.14) + (3.15) we can see that we are not actually in need of computing the integral of Φ if we have the two integrals in (3.12). Then dividing by the right denominator we get the solution of Φ except for the missing part (3.15). This shows that the two integrals does actually determine the system.

3.1 The linear velocity case

Paper [5] has discussed the linear velocity case. Here we are going to examine the special case where $\vec{X}(t) = \vec{v}t$. To get a better overview we split solution (3.11) into the two integrals, while also making sure to remove the part dependant on t. The minus is dropped so that the solution is $I_1 - I_2$. Noteworthy in this case since there are no rotations involved we can also relax the requirements and include pressure distribution that are not rotationally invariant, e.g a rectangularly shaped load/pressure distribution presented later on.

$$I_1(t) = \frac{G_0 w_0 e^{-t(R-iU)}}{2iU}\int_0^t e^{\tau(R-iU)-i\vec{v}\tau\cdot\xi} d\tau \tag{3.16}$$

$$I_2(t) = \frac{G_0 w_0 e^{-t(R+iU)}}{2iU}\int_0^t e^{\tau(R+iU)-i\vec{v}\tau\cdot\xi} d\tau \tag{3.17}$$

When the linear velocity is introduced the integrals becomes an exponential function with a linear exponent in τ. Therefore we are left with the two solution integrals:

$$I_1 = \frac{1}{(R - iU - i\vec{v}\cdot\xi)}\left(e^{t(R-iU)-it\vec{v}\cdot\xi} - 1\right) \text{ and } I_2 = \frac{1}{(R + iU - i\vec{v}\cdot\xi)}\left(e^{t(R+iU)-it\vec{v}\cdot\xi} - 1\right)$$

Finally substituting them back together, and simplifying the expression as follows:

$$-\frac{G_0 i}{2U}\frac{\bar{f}}{k}(\xi)\left(e^{-t(R-iU)}\int_0^t e^{\tau(R-iU)-ia(\tau)\xi}d\tau - e^{-t(R+iU)}\int_0^t e^{\tau(R+iU)-ia(\tau)\xi}d\tau\right) \tag{3.18}$$

$$= -\frac{G_0 i}{2U}\frac{\bar{f}}{k}(\xi)\left(e^{-t(R-iU)}I_1(t) - e^{-t(R+iU)}I_2(t)\right) \tag{3.19}$$

$$= -\frac{G_0 i}{2U}\frac{\bar{f}}{k}(\xi)\left[e^{-t(R-iU)}\frac{\left(e^{t(R-iU)-itv\cdot\xi} - 1\right)}{(R - iU - iv\cdot\xi)} - e^{-t(R+iU)}\frac{(e^{t(R+iU)-itv\cdot\xi} - 1)}{(R + iU - iv\cdot\xi)}\right] \tag{3.20}$$

$$= -\frac{G_0 i}{2U}\frac{\bar{f}}{k}(\xi)\left[\frac{\left(e^{-itv\cdot\xi} - e^{-t(R-iU)}\right)}{(R - iU - iv\cdot\xi)} - \frac{(e^{-itv\cdot\xi} - e^{-t(R+iU)})}{(R + iU - iv\cdot\xi)}\right] \tag{3.21}$$

To achieve the solution presented in [5] we take apart the solution and look at the different parts separately. If we look at the parts involving: $e^{-t(R+iU)}$ and $e^{-t(R-iU)}$ we can extract:

$$= \frac{G_0 i\bar{f}}{2U}\frac{1}{(R + iU - iv\cdot\xi)}e^{-Rt-iUt} \tag{3.22}$$

for the first part and for the second part:

$$= -\frac{G_0 i}{2U}\frac{\bar{f}}{k}\frac{1}{(R - iU - iv\cdot\xi)}e^{-Rt+iUt} \tag{3.23}$$

Then we go onto parts involving $e^{-i\vec{v}t\cdot\xi}$ in brackets in expression (3.21), finding the common denominator:

$$-\frac{G_0 i}{2U}\frac{\bar{f}}{k}e^{itv\cdot\xi}\frac{(R - iU + iv\cdot\xi) - (R + iU + iv\cdot\xi)}{(R - iU + iv\cdot\xi)(R + iU + iv\cdot\xi)} \tag{3.24}$$

$$= -\frac{G_0 i}{2U}\frac{\bar{f}}{k}\frac{-2Ui}{(R - iU + iv\cdot\xi)(R + iU + iv\cdot\xi)} \tag{3.25}$$

$$= -\frac{\bar{f}}{k}\frac{G_0}{(R - iU + iv\cdot\xi)(R + iU + iv\cdot\xi)}e^{itv\cdot\xi} \tag{3.26}$$

If we now exclude the exponential terms, the equation (3.22,3.23,3.26) corresponds to the A_η, B_η, C_η in [5] respectively. We have hereby shown that our solution is the generalization of the solution presented in [5].

3.2 Numerical methods

After solving the integrals, we compute the inverse Fourier transform, here done by the Fast Fourier method (FFT). The difference from the continuous transform is that we are now dealing with a periodic solution on an infinite ice sheet instead of a single solution. One could look at it as if there are infinitely many moving cars spaced with distance l to the next vehicle in each of the coordinate axis. If the radius is large the influence of the other loads will be minimal, and we are left with a good approximation of the true solution. Since we are on a finite domain we are no longer talking about a continuous frequency/wave domain, but a discrete one where $k(n) = \frac{n\pi}{l}, n \in \mathbb{Z}$. For computational sake, we are approximating this with a finite subset of $\mathbb{Z}$. Of course this needs to be extended to the 2D Fourier transform by considering the vector $k(\vec{n}) = [k_1(n), k_2(n)]$ and where $n = [n_1, n_2]$.

For $\eta(x, t)$ a direct Dirac distribution will converge towards a solution. However, when we start computing the strain we ran into a problem. The approximated strain is computed from the second-order derivatives; in Fourier terms, we multiply by $-k_1(n)^2$ to get the ∂_{x_1} operator. If we try to keep the Dirac distribution the result will not converge properly for the whole domain. The answer to this problem is to use a Gaussian; this will make the strain converge well. It also makes physical sense that if a finite load is distributed over a 0 area point; the pressure at that point will be infinite.

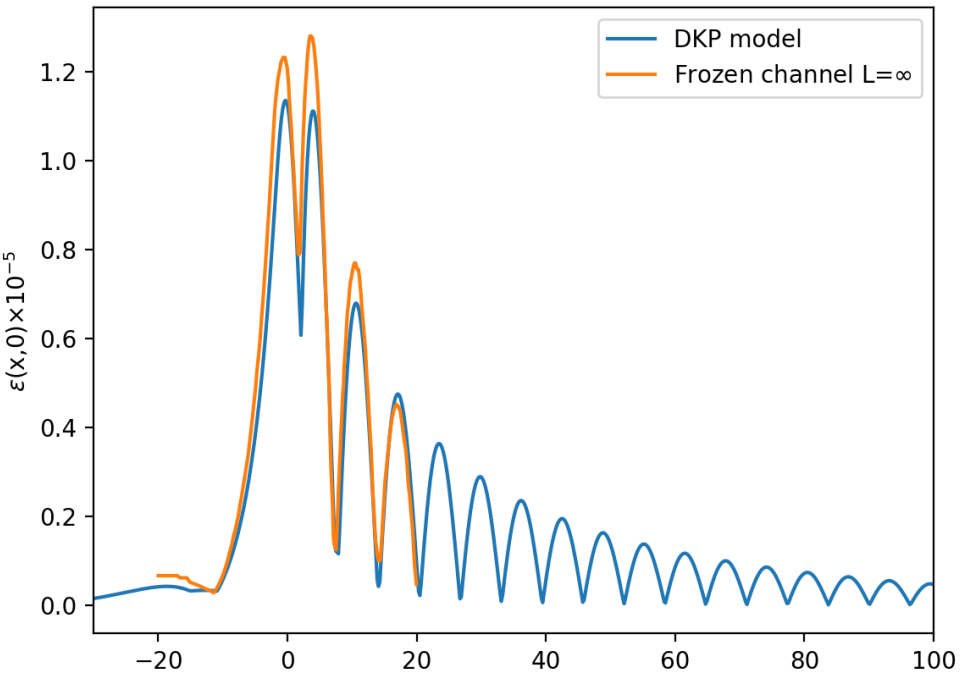

Figure 3.1: Strain measurement along central line compared to alternative model

In this picture we have used the linear velocity solution, the blue line is the Main Model (3.21), for the linear case. This model is run with the same weight as in [17]. Here we have compared the two results of the strain. The parameters used in both cases where H = 2 m h = 0.1 m v = 7 m/s, E = 4.2e+9. And a pressure force totalling to $P_0 = 1kN$. There are some discrepancies but as they are different models one should expect such.

If we compare this with the strain shown in the [17] paper it lines up quite well for the central line $\varepsilon(x, 0)$ on the right-hand picture.

The last thing is the integration procedure. If we have a path $X(t) = X_1(t), t < c, X_2(t), t > c$ with two parts, say a straight path followed by a turn. Then it may be convenient to use the split up solution of (3.11). Because we can integrate the pieces separately and then glue them together to get a full solution. If we want a part of the first solution we only need to integrate over X_1 but if we afterwards want the

$$\frac{G_0 w_0}{2iU}\left(\int_0^t (e^{-(t-\tau)(R-iU)}e^{iX(\vec{\tau})\cdot\xi}d\tau - \int_0^t e^{-(t-\tau)(R+iU)}e^{iX(\vec{\tau})\cdot\xi}d\tau\right) \tag{3.27}$$

If we now define the two integrals over $X_1(t)$ as.

$$I_1 = \int_0^c (e^{-(t-\tau)(R-iU)}e^{iX(\vec{\tau})\cdot\xi}d\tau, \quad I_1 = \int_0^c (e^{-(t-\tau)(R+iU)}e^{iX(\vec{\tau})\cdot\xi}d\tau \tag{3.28}$$

Then the final solution can be written as:

$$\frac{G_0 w_0}{2iU}\left(e^{-(t-c)(R-iU)}I_1 + \int_c^t e^{-(t-\tau)(R-iU)-iX(\vec{\tau})\cdot\xi}d\tau - e^{-(t-c)(R+iU)}I_2 - \int_c^t e^{-(t-\tau)(R+iU)-iX(\vec{\tau})\cdot\xi}\right) \tag{3.29}$$

This can be turned into an iterative process if one needs the solution for the whole time evolution. Another way to do this is to compute $\Phi(x,t)$ and use the previous solution as initial conditions, and propagate the solution that way. An example of the integral method is in the first contour plots in the next section fig:4.3 where a straight path is followed by a circular one.

It is also possible to use a linear approach to find the solution where we assume that the vehicle is moving linearly between points. That would be similar to assuming that the integrals are just exponentials with linear exponents in t. That could also be used in the numerical treatment in [5].

Chapter 4

Results

In this section, we will investigate and analyse the results from our model. Comparing them to real-world data from the field report[20]. And we will have a look at circular path solution to 3.11. We will examine the properties of the model and compare it to the real physical experiments.

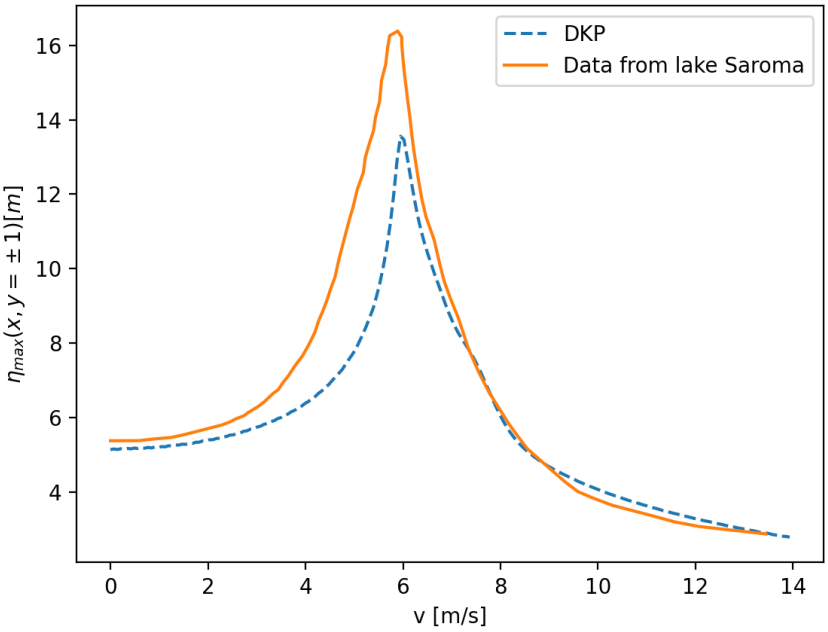

Figure 4.1: Comparing the maximum ice depression of the DKP model to the Takizawa filed report data

The DKP model is compared to a curve fitting the field data presented in the field report [20] [figure 9].Same as in figure 4.2 $B = 0.1$ and the load is a rectangle of dimensions $2.43m \times 0.79m$ with a weight/(total force) of 235kg[21]. In the model the weight is assumed to be spread uniformly inside of the area and the snapshot is taken after t = 100 s. Then the measurement is taken to be the max of the amplitude of all the points taken 1 m in transversal distance from the load. The only difference between the model data and the physical experiment is that data collection was measured as the max of a time series.

While the top does not reach as high as in the field studies the graph is shaper than in [20].Now here the B value has been set to 0.1 like in [20] to get the best fit for the max amplitude. While later in the article a value of B = 0.41 is used as that seems to give a better fit for the wave speed. But either way the model well predicts the max amplitude to either side of the critical speed. The next thing to look at is the max strain in the ice. We let the load move with linear velocity for a certain time and then find the maximum strain, for different velocities.

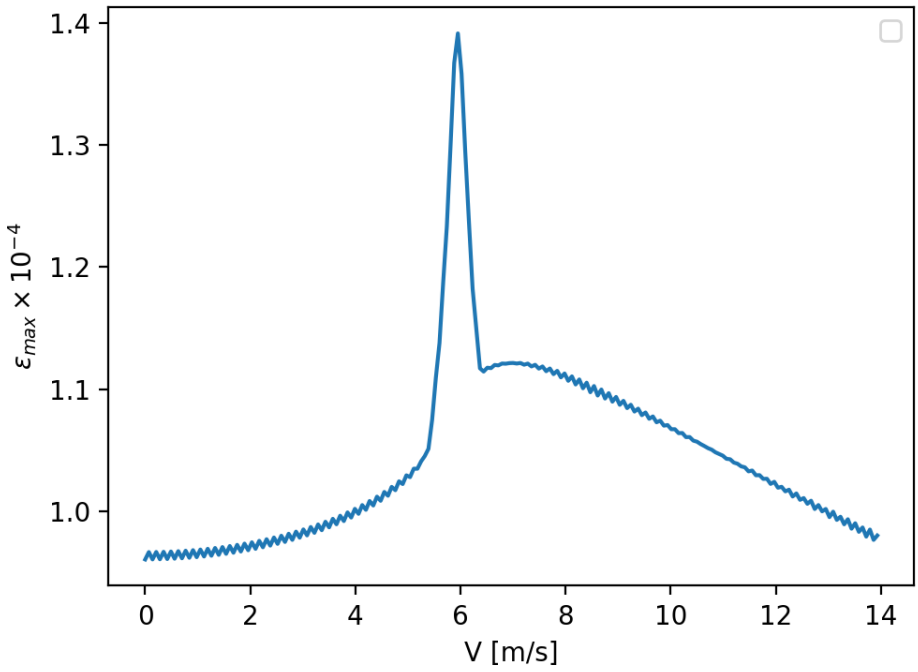

Figure 4.2: $\varepsilon_{max} \times 10^{-4}$ as a function of velocity, after $t = 100s$

This figure shows the maximum strain measured at t = 100 for different speeds. We can see that the maximum is reached when the velocity is around the critical speed $u_c \approx 6.1m/s$. The parameters are from Lake Saroma in figure 2.2 Same as inf figure4.1 $B = 0.1$ and the load is a rectangle of dimensions $2.43m \times 0.79m$ the weight was 235kg [21]. The load is simulated as a uniform rectangular pressure distribution.

As we can see strain follows a similar pattern to amplitude. The max strain is reached around the critical speed before going down again. We can also so that in contrast to the amplitude the strain does not decrease as fast after the critical speed. This was also touched upon in chapter 3 3.1 which shows a typical central line of the strain.

4.1 Circular case

Looking at the differences in the wave profile between the circular and linear cases, we wnalysing the case when H = 6.8 h = 0.17. Here the $v_c = 6.1$ m/s, the same case as in [20]. This is run as one simulation where we start from a linear path and then go into a 40 m radius turn.

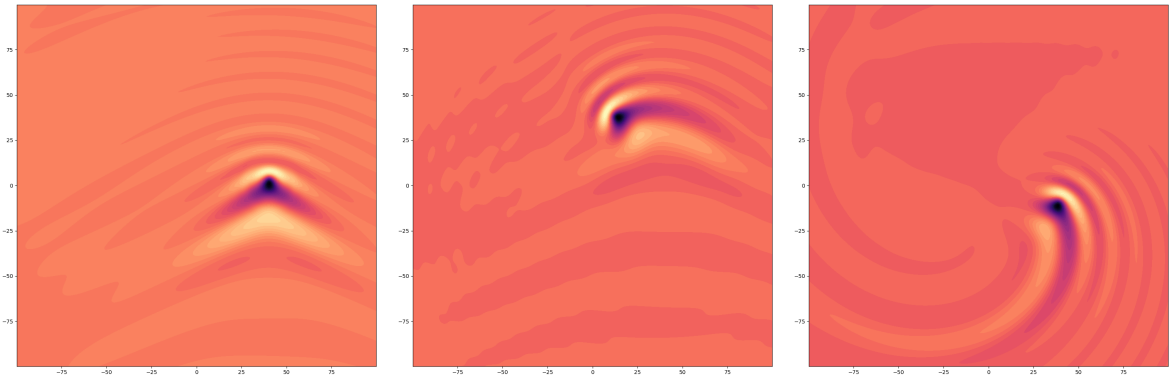

Figure 4.3: Circular path contour-plot with linear velocity path as initial condition

left: shows the part before the turn has made much effect t = 0.5s. center: is while the wave patterns are transitioning to the turning case, t = 7.3s. right: After some time we get a semi stable case t = 34.5s where we have a characteristic wave profile around the load. And a spiralling wave emanating from the load moving out of the boundary, which we will have a better look at later.

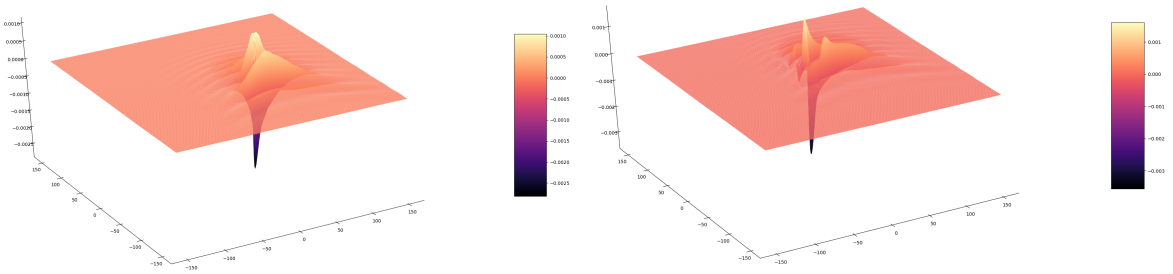

Figure 4.4: 3-D plots of circular path

Circular path with linear velocity case as initial condition. Corresponding to the contour plots t= 0.5 and t= 7.3. t = 34.5 is in fig 4.5. 4.3

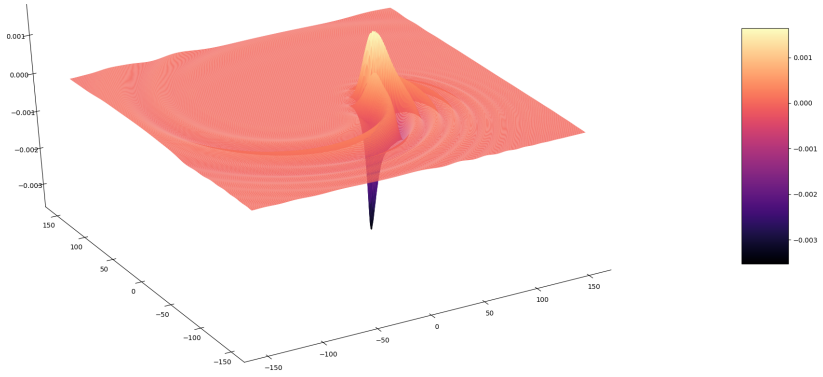

Figure 4.5: 3-D plot of circular path

Circular path with linear velocity case as initial condition. 3-D plots corresponding to contour plots 4.3 for t = 34.5.

In plot 4.6 the max strain and amplitude is measured for the whole time series. Note that the max amplitude is usually going to be directly or close to or directly underneath the moving load.

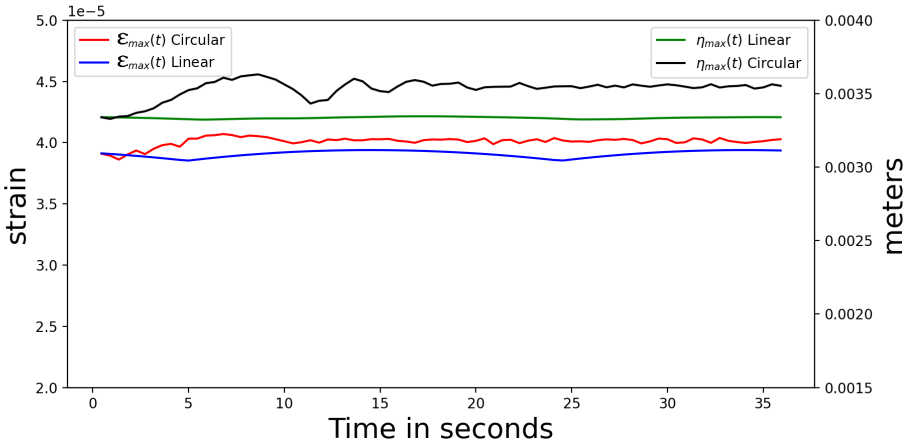

Figure 4.6: Plotting of stress circular path vs linear path

Here we have plotted the case from above, both amplitude η and strain ε for the circular case presented in fig: (4.3,4.4,4.5) compared to a load just continuing travelling in a straight line. The red and blue plots are the strain and the black and green are the amplitude.

Both the strain and amplitude are larger for the circular case and there is a small hump in the end suggesting that there is some constructive interference. But this is not a significant difference from the regular case. The difference will increase if we have a sharper turn, but only for turns well beyond what would be possible.

One final note is on the stability of the solution one way of determining this is to look at one of the axis in space and the other in time. If we do this we get the solution as follows.

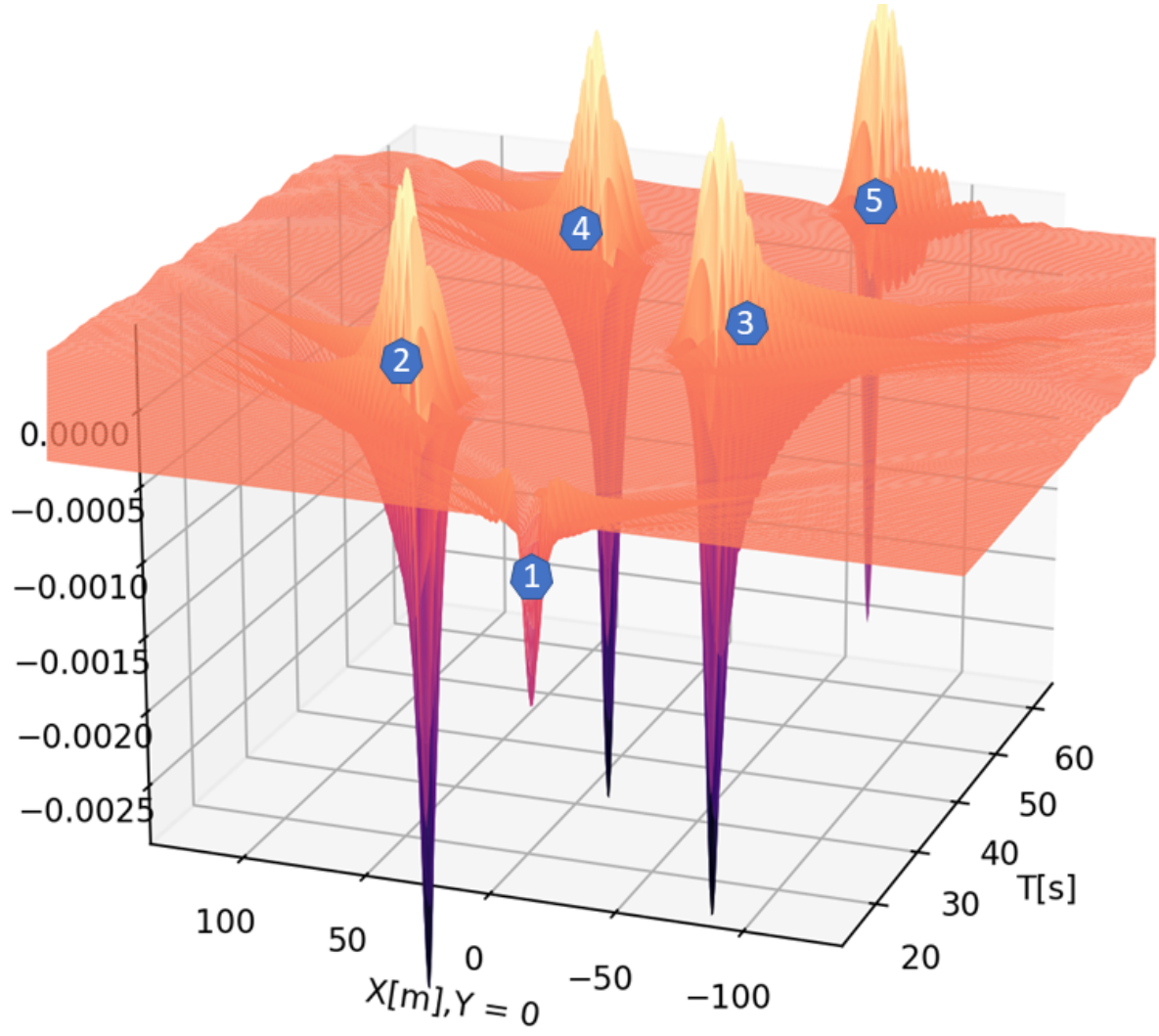

Figure 4.7: plot of amplitude along the x axis for different times t

In this experiment we have used the same case as in figure 4.3,4.4,4.5, but we have plotted the x axis of the solution at different times t $\eta(x, y = 0, t)$ .As we can see the solution is periodic with some wave travelling outside of the boundary and being reflected back. The solution starts of well,the only problem starts after two turns, then the reflections from the boundaries starts to influence the solution. However this is almost negligible especially when looking at the amplitude profile close to the load. This fact needs to be considered when deciding on the size of the computational domain. Each of the spikes numbered here is when the load passes the x-axis. They are on both sides as the load will go around and pas the X-axis on the other side.

As we can see in figure 4.7 the solution follows a steady pattern but in the end one gets a reflection from he boundaries. As the reflection of the waves are due to the numerical method this is not something we can consider a part of the solution. In the end at the leftmost spike we can see the solution is actually affected by a bit by the reflections, though the main spikes, of which there are five including the initial spike at the front to the right, are almost unaffected. This is due to the damping of the solution which in

this case could be considered high B=0.41. In the next chapter 5 we are going to see an alternative method of solving this system that mitigates some of the boundary problems, though it ads some new ones.

4.2 Different distributions, the rectangular case

Next, we are going to look at how the model behaves as a result of different pressure distributions, effectively changing w_0 in 3.9 where we are going to look at $P(x, y, t) = 1, (x, y) \in D$ where D is a rectangle. There are two cases we will look at inspired by [12] where they look at at a rectangle with varying side lengths.

Starting with the rectangle of dimensions 40 by 4 meters with the short side toward the direction of travel as shown in the picture 4.8.

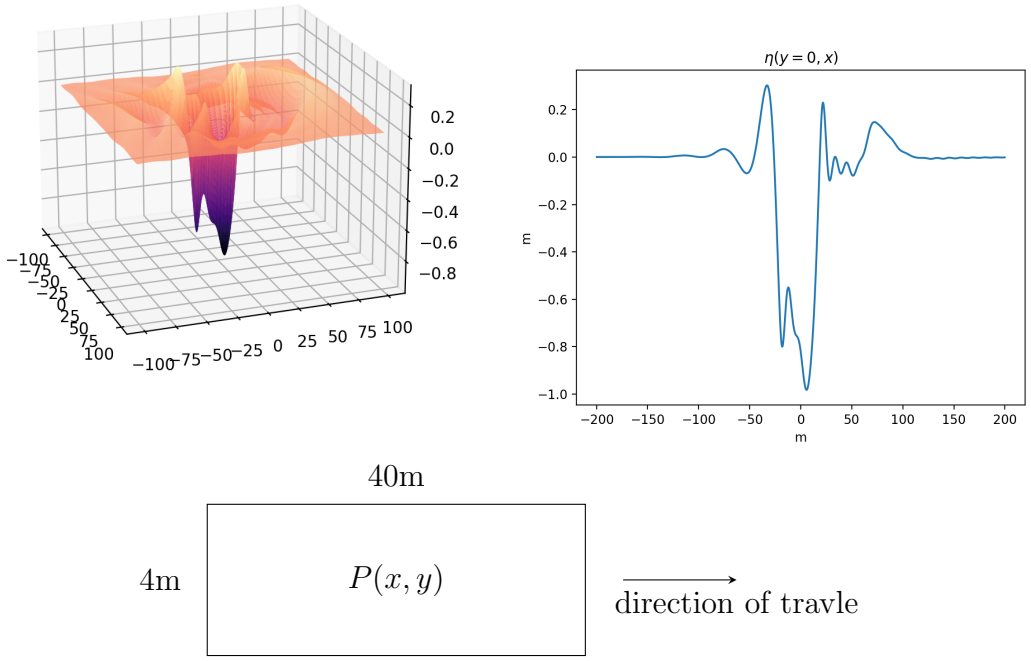

Figure 4.8: Rectangular (40m x 4m) shaped pressure distribution travelling over the ice, short side towards the direction of travel

The load is travelling to the right with velocity $v = 6.5m/s$. The center of mass is positioned at (x,y) = (0,0) Left: Full 3D plot, right: central line of the 3D plot to the left. All of the measurements are in meters and the coefficients used are from the "Lake Saroma" in table 2.2.

The next is to look at the opposite case where the long side is towards the direction of travel.

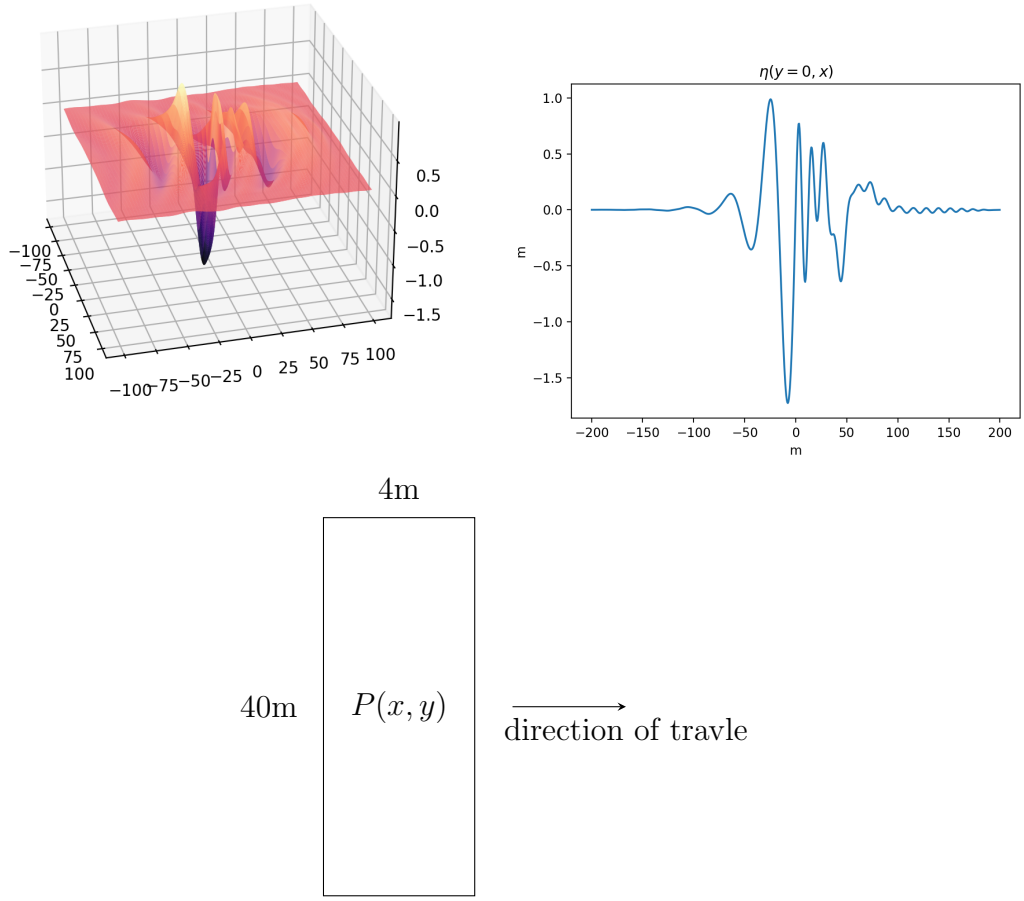

Figure 4.9: Rectangular (4m x 40m) shaped pressure distribution travelling over the ice, long side towards the direction of travel

The load travelling to the right with velocity $v = 6.5m/s$. The center of mass is positioned at (x,y) = (0,0). Left: Full 3d plot of the amplitude $\eta(x, y)$, right: central line $\eta(x, y = 0)$ The weights is the same as in the previous case: 4.8

these scenarios where also tested for non-symmetrical pressure distribution, like a triangle added below, but these become more difficult to analyse.

For comparison, the first thing we can note is that the amplitude of the pressure distribution with its long side facing the travelling direction seems to generate a lot higher waves than the rectangle facing the opposite side, though the lowest part of η seems more comparable between the two solutions 4.8,4.9.

4.3 Convergence of the solution when using a delta distribution

In this section, we are going to have a look at what happens to the solution, when $P(\vec{x}, t) = \rho\delta(\vec{x} - \vec{X}(t))$. This distribution can only be represented as a limit function with say a Gaussian of constant integral. But it has a Fourier transform 1 possibly depending on where the load is placed and the convention of the Fourier transform. We are only going to look at it in the linear case to illustrate a problem with measuring the stress in the ice. And why we can use a delta distribution when we are only interested in the amplitude, but not when we need the strain.

Starting with the amplitude to show the convergence of the solution we have represented the amplitude under the load 4.10, and the maximum amplitude per n where n is the number of grid points. The total solution domain is set to 800 by 800 meters and where tested for $m = 200$ 600 and 3200. Where the number of grid points are n^2

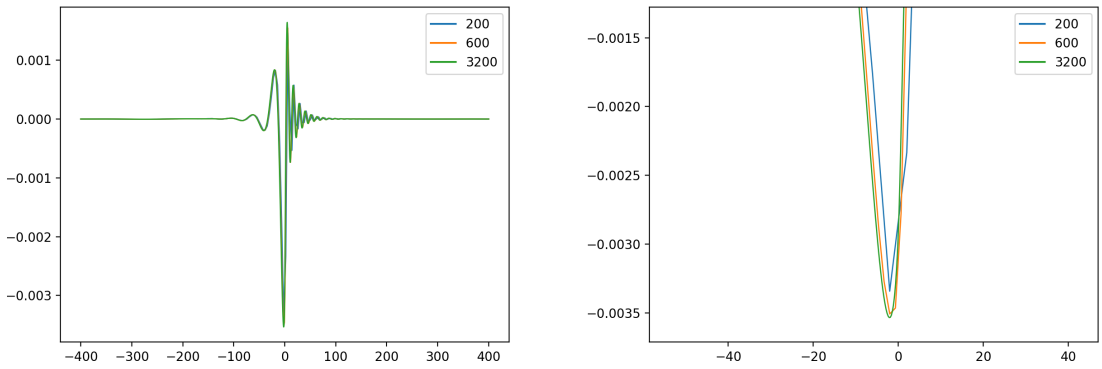

Figure 4.10: Shows the central line of η of the plots for the different number of grid points m

As we can see in 4.10, using a delta distribution we get a convergent solution.

But in the stress case, its not so. We need to multiply with ξ twice to get the derivatives in the Hessian matrix to get the strain. We can see that the max strain converges everywhere, except for the spike right in front of the load. However as the most important information is the maximum strain, as that is what breaks the ice, we need this to be convergent as well.

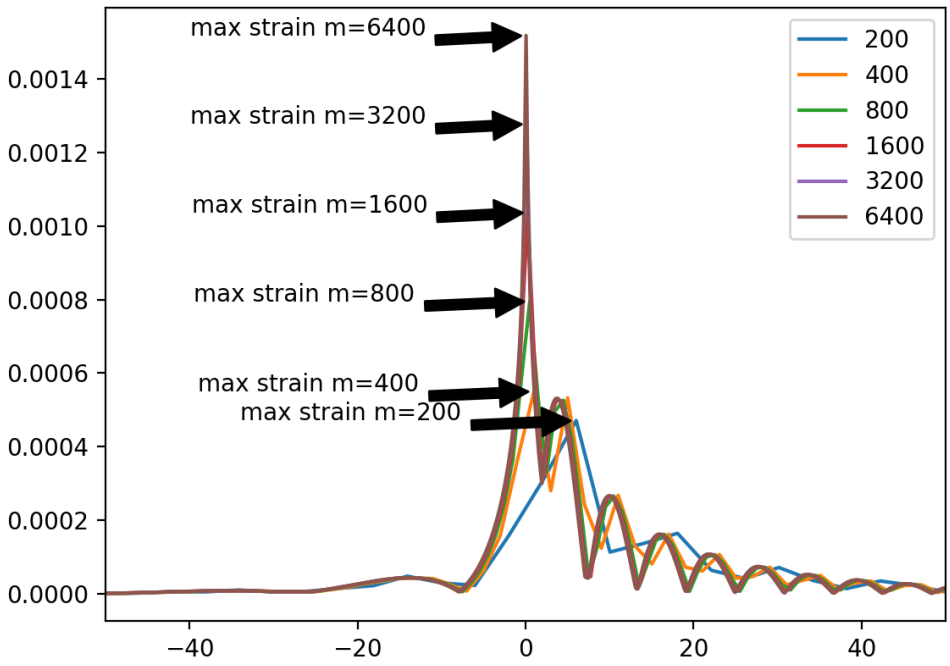

Figure 4.11: Shows the central line of the plots for the different values of m

If we use a gaussian or a non point load in stead then the strain will also converge as we have seen in the previous chapter 3 3.1

4.4 Driving a car on the ice while trying to avoid an obstacle

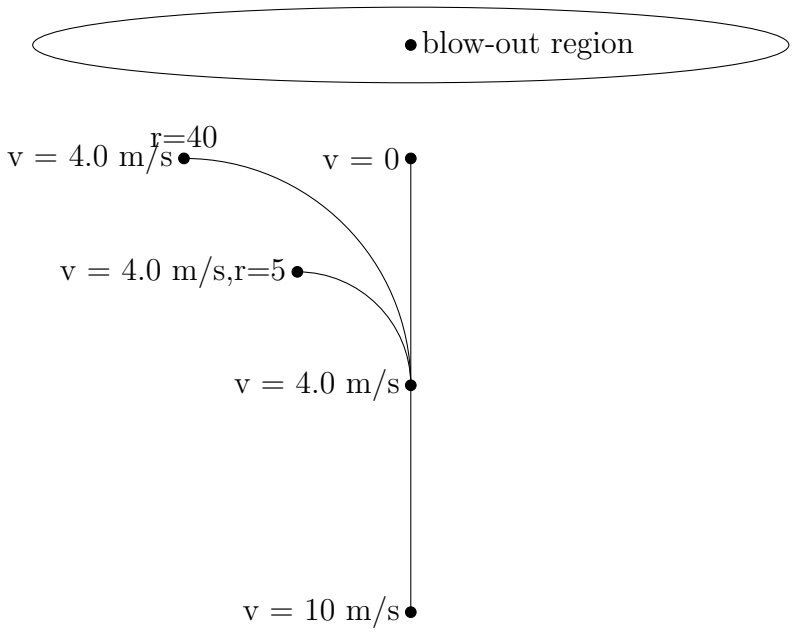

The experiment starts with a change in water depth from 25 m with and an ice thickness of 0.7 m to a 1 m water depth and 0.2 m ice thickness. This change would effectively drop the critical speed from 10.43 m/s to 3.13 m/s. If a car starts off driving at 10 m/s, something that would be safe in the first part, will now be well beyond the critical speed in the last case. If there is now a blow-out region in front, as can often happen in such areas with sudden drops in critical velocities due to previous cars, one would want to avoid the blow-out region. This can manly be done in two ways, by turning or slowing down. We are going to start all the cases with slowing down from $10m/s$ to 4 m/s = 14.4 km/h. Then there has to be made a decision either turn immediately while driving at $4m/s$, and not slow down further. Or slow down to a stop before the dangerous area. But, because of the decreasing depth, the critical speed has now decreased to 3.13m/s = 11.3 km/h which you are now way beyond, in relative terms. The initial condition for the experiments is a load moving at $10m/s$ in the last case (H=1,h=0.2).

After running the experiment we measure the strain on the ice-sheet for different times and plot the maximum for that time. Afterwards the cars are left turning to see how it is stabilising, but the results are stabilising well before the cars are out of the turn. Of the cases shown in the plots below the most dangerous one seems to be turning too early with a large radius (r=40,r=80). These paths puts a lot more stress on the ice over a greater time. The only exception is the 5-meter turning radius case where the strain decreases and actually falls bellow the deceleration case. However, as traction will always be a problem when driving on ice a 5-meter radius might be infeasible. Therefore you might have to resolve to a turn with a larger radius leaving you in the same case as

above. If you slow down until you are below the critical speed then you are out of harm's way. But will you be able to avoid the dangerous area then?

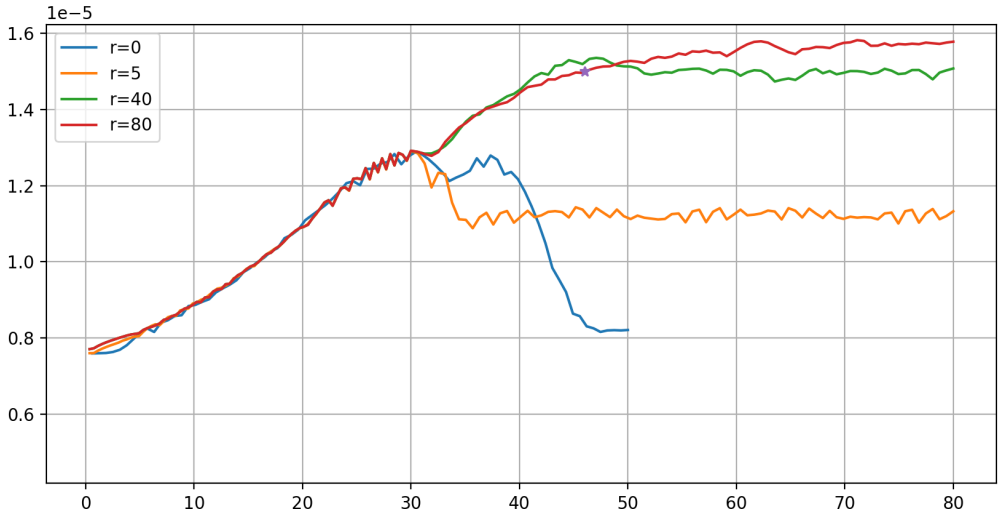

Figure 4.12: Comparison of stress for different paths

For this experiment the following variables were used H= 1 , h = 0.2, and for the rest the as in "Lake Samora" 2.2. The initial conditions t = 0 are created by letting a car move at 10 m/s for 20 sec. Then the car slows down from t = 0 to t = 30 after t = 30 the car either starts turning with (r = 5,40,80) or slows down r = 0. The cars turning are left turning after making the turn to see when the maximum is reached. For all turning cases a steady state is reached well before the turn is over.

Concluding, strain is significantly increased when one is choosing to turn instead of slowing down, unless one are turning really sharply. This may lead to a disastrous result.

Chapter 5

An alternative transform method in space, The Hankel transform

This part will give an alternative formulation of the problem in polar coordinates and show how one can use the Hankel transform to solve the PDE system (2.22,2.23). In addition we will use a numerical solver for this transform method the quasi discreet Hankel transform. This numerical solver uses a logarithmic variable change to solve the Hankel transform via the (FFT) method, so the computational speed should be comparable.

5.1 Transform methods

A general way of looking at a Transformation method is by defining it as an operator $T[f]$ acting on a function $f(x)$, defined by the integration kernel $K(\xi, x)$ and the integration domain ω in the following way [3].

$$T[f] = \int_{\omega} f(x)K(x,\xi)dx \tag{5.1}$$

If certain criteria are satisfied by the kernel K, the operator T, and only a suitable space of functions f are considered. Then the transform can be injective and possibly also surjective. The advantages of these transformations are clear if we look at differential equations. Usually differential equations are defined by one or more differential operators L; if we take the transform of f with the operator L we get $T(L(f)) = \int_{\omega} L(f)K(\xi, x)dx = \int_{\omega} fL(K(\xi, x))dx$ plus some boundary terms. These boundary terms may vanish if the

kernel or the functional space f is of a suitable type. If then the differential operator when acting on the kernel becomes something "nice" along the lines of $L(K) = M(\xi)K(\xi, x)$ then we are left with:

$$T(L(f)) = \int_{\omega} fK(\xi, x)M(\xi)dx = M(\xi)T(f) \tag{5.2}$$

We can now see that if we have an inverse of the transform denoted by $T^{-1}(f)$ the solution of the differential equation becomes:

$$L(f) = T^{-1}[M(\xi)T[f]] \tag{5.3}$$

If the inverse is computable then this should only be an algebraic computation, in stead of a differential equation.

We are going to look at the case when the kernel is based on the Bessel functions. A Bessel function $J_\alpha(x)$ of order $\alpha \in \mathbb{R}$, can be defined as the solution to the ordinary differerential equation

$$x^2\frac{d^2J_\alpha}{dy^2} + x\frac{dJ_\alpha}{dx} + (x^2 - \alpha^2)J_\alpha = 0 \tag{5.4}$$

If we make a coordinate transformation of the Laplace operator in 2 dimentions from rectilinear coordinates (x,y) $\triangle = \partial_x^2 + \partial_y^2$ to polar coordinates (θ, r) we get the following expression:

$$\frac{\partial^2 u}{\partial r^2} + \frac{1}{r}\frac{\partial u}{\partial r} + \frac{1}{r^2}\frac{\partial^2 u}{\partial \theta^2} \tag{5.5}$$

The next step is to expand the function $\eta(r, \eta, t) = \sum_n c_n(r, t)e^{in\eta}$. Taking the derivative with respect to η the result becomes the same as multiplying by (in). In terms of the Laplace equation we get the sets of ordinary differential equations.

$$\sum_n \left(\partial_r^2 c_n(r, t) + \frac{1}{r}\partial_r c_n(r, t) + \frac{n^2}{r^2}c_n(r, t)\right) e^{in\phi} \tag{5.6}$$

The next thing is to introduce the transform in the same way we defined a general transform method in 5.1. By this definition the Hankel transform of order v, for a suitable function or distribution f, is given by:

$$\mathcal{H}_v(f)(k) = \int_0^\infty rJ_v(rk)f(r)dr \tag{5.7}$$

The requirements of the function f is that f has either to be compactly supported or go "fast enough" to zero as $r \to \infty$. We also want f to be an integrable distribution or function such that $\int_0^\infty |f(r)|r^{1/2}dr < \infty$ [14].

Then looking at the Laplace operators in the Hankel transform space. Following broadly the same approach as in [2] and [14].

$$\begin{aligned}\int_0^\infty rJ_n(rk)\triangle_n f_n(r)dr &= \int_0^\infty rJ_n(kr)\left(\frac{\partial^2}{\partial r^2}+\frac{1}{r}\frac{\partial}{\partial r}+\frac{1}{r^2}\frac{\partial^2}{\partial\theta^2}\right)[f(r)_n]dr \\ &= \int_0^\infty J_v(kr)\left(\frac{\partial}{\partial r}r\frac{\partial}{\partial r}-\frac{n^2}{r}\right)[f_n(r)]dr = \\ \int_0^\infty \left(\frac{\partial}{\partial r}r\frac{\partial}{\partial r}-\frac{n^2}{r^2}\right)[J_n(rk)]f(r)dr &+ J_n(rk)r\frac{\partial}{\partial r}f(r)\Big|_0^\infty + \frac{\partial}{\partial r}\left[J_n(rk)r\right]f(r)\Big|_0^\infty \\ &= -k^2\int_0^\infty J_n(rk)f(r)rdr = -k^2\mathtt{H}_n(f(r))\end{aligned}$$

This can also be justified recursively for the Laplace operator in higher order $\triangle^n = (-k^2)^n$. Now since our system is linear in η and Φ we can expand them into the Fourier series in θ such that $\eta(r,\theta,t) = \sum_n \eta_n(r,t)e^{in\theta}$. And lets us define the operators $G_{0,n} =$

$$G_{0,n} = \sqrt{-\triangle_n}\tanh(H\sqrt{-\triangle_n}) \tag{5.8}$$

and

$$K_n = 1 + \frac{h\rho_I}{\rho}\left(1-\frac{h^2\triangle_n}{12}\right)G_{0,n} \tag{5.9}$$

The first stage now is to expand the solution $\eta(r,\theta,t) = \sum_n \eta_n(r,t)e^{in\theta}$. Then insert this into the set (2.22 2.23):

$$\sum_n \eta_{n,t}e^{in\theta} = G_0\sum_n \Phi_n e^{in\theta} \tag{5.10}$$

$$\sum_n \Phi_{n,t}e^{in\theta} = \sum_n \left(-g\frac{1+\chi\triangle^2}{K}\eta_n - \frac{b}{\rho}\frac{G_0}{K}\Phi_n - w_n\right)e^{in\theta} \tag{5.11}$$

Now as this is just a regular Fourier expansion we know that the exponential basis is an orthogonal basis thus this should hold for each term n. We can therefore exchange the operators $G_0, K, \triangle$ for our counterparts 5.8,5.9,$\triangle_n$ yielding us the following n sets of

ordinary differential equations in r:

$$\eta_{n,t} = G_{0,n}\Phi_n$$
$$\Phi_{n,t} = -g\frac{1+\chi\triangle_n^2}{K_n}\eta_n - \frac{b}{\rho}\frac{G_{0,n}}{K_n}\Phi_n - w_n$$

Now from the previous equations we know that $\triangle_n = -k^2$ if we use the n-th hankel transform so let us just apply the hankel transforms in order and we are left with all the same operators but different transforms.

$$\mathcal{H}_n(\eta_{n,t}) = \mathcal{H}_n G_{0,n}\Phi_n \tag{5.12}$$
$$\mathcal{H}_n\Phi_{n,t} = \mathcal{H}_n\left(-g\frac{1+\chi\triangle_n^2}{K_n}\eta_n - \frac{b}{\rho}\frac{G_{0,n}}{K_n}\Phi_n - w_n\right) \tag{5.13}$$

Now as in the Fourier case we are left with set of algebraic equations that is solvable. Conveniently the solution follows closely the linear velocity solution, but we need to exchange $-\|\vec{\xi}\|^2$ for k^2. To retrieve, the solution we need to solve the algebraic terms and then take the inverse Hankel transform of the same order for each of the n equations. Finally we take the inverse Fourier transform in the θ parameter. For this to be useful we have to find a way of numerically solving the Hankel transform. A possibility is to employ the Quasi Fast Hankel transform, conveniently available from the scipy library released in (2021).

5.2 Hankel-transform using Quasi Fast Hankel Transform (FHT)

Here we use the Scipy version of the Quasi Fast Hankel Transform from the scipy liberary, wich uses the approach described in [22],[7] As this transform in our case can only be used for purely circular paths with linear velocity, that will be the only case we will look at. Setting $v = 6.5m/s$ and the rest of the variables form "Lake Samora" 2.2 gives the following results:

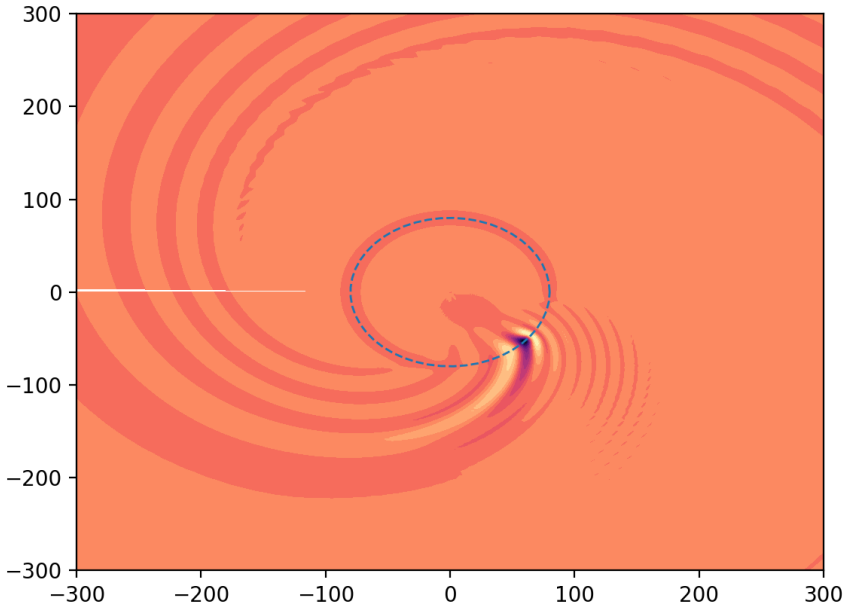

Figure 5.1: Hankel transform contour-plot close up

Hankel transform solution using "Lake Samora" from 2.2. With v = 6.5 m/s and t = 736s. The blue dotted circle marks the path of the load

If we look at a larger area get the following picture 5.2. We can see the waves travelling away from the load in a spiralling patterns emanating from the load.

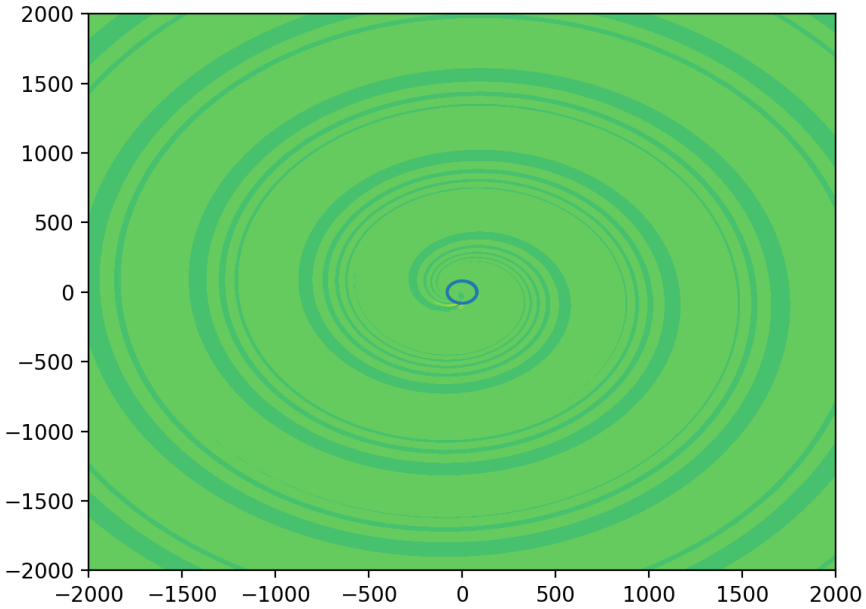

Figure 5.2: Hankel Transform 2

let go for t = 736s that is over 10 rounds around the center same coefficients as in 5.1, the small blue circle indicates the path of the load.

Now this look similar to (4.4,4.3), but there is a slight problem with the amplitude close to $r = 0$, unfortunately where the load is placed.

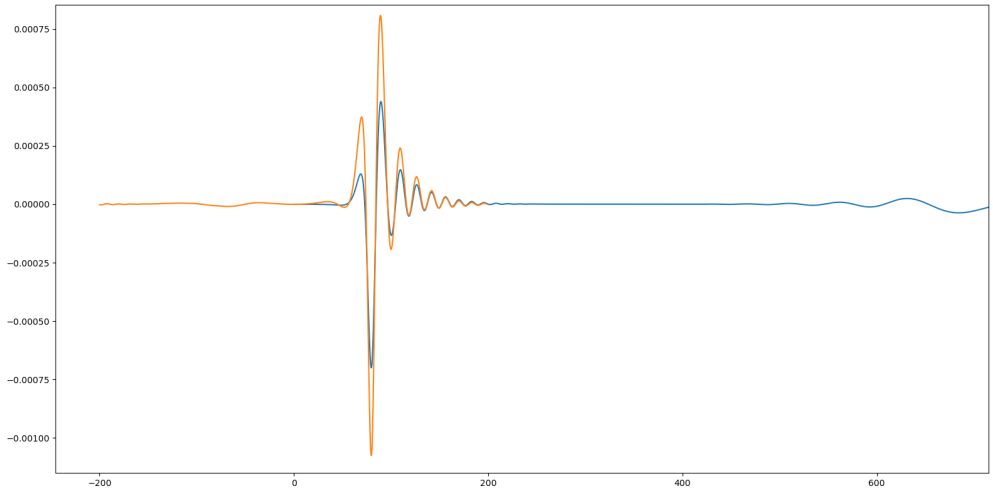

Figure 5.3: Comparison Hankel transform and Fourier transform

Hankel and Fourier transform: The blue line is the Hankel transform solution and the orange is the Fourier transform. To get the solutions to match the load was placed at one of the coordinate axis which also corresponded to one of the angles in the polar plot. Then plotting the solution $\eta(\phi = 0, r)$ and $\eta(x, y = 0)$. The domain of the Hankel transform was much larger than the Fourier transform

First the wave length and wave speed are coinciding quite well. We can see in 5.3 the Hankel transform underestimates the amplitude close to the center of the circular path. However, the solutions seems to converge when further away from the origin. This may or may not be a problem, depending on what we are looking for. If we are looking for the large scale influence and wave patterns further away from the center of the circular path, the model may still gives an accurate prediction. As well as an interesting wave pattern as shown in 5.2. One of the uses for this solution could be to inversely approximate parameters and properties of the ice in another way. An example of this could be the damping coefficient, if we placed a set off measurement points in a line way from the origin we should be able to predict the time the wave has travelled before reaching that point, as the wave is roughly going in a tangential path to the moving load when it is created.

As an extra note it is also possible to use a quadrature solver for the Hankel transform but that would be slower and usually has a hard cap for the order v of the transform. For those reasons it was not included in this thesis. An exhaustive research was not done into quadrature solvers and one could find solvers that may work better, yielding a better result also closer to the load.

Chapter 6

Summary and further work

Following steps outlined in the thesis we have shown how to get to the linearized Partial differential equation system (2.21,2.22) from the basic fluid and continuum mechanical laws and models. How critical speed is defined and also how different speeds affect the solution; we have shown that driving with a speed close to the critical speed gives the largest amplitudes.

In chapter two we solved the system of partial differential equations (2.21, 2.22), showing that this set has a well-defined solution (3.12) defined by an integral. A solution that in the linear velocity case coincided with the solution presented in [5]. Also, that it could be considered an extension of that solution [5]. In the end, we also looked at the strain. Here our solution was in good agreement with [16] who used another model.

Examining amplitude data in chapter three, we found that the amplitude was in good agreement with the max amplitude data from [20]. Next step was looking at different solutions for the circular path 4.10. We could conclude that how the strain acted, is not significantly affected by the radius of a turn in the normal range. It needs additional mention that our solution here is to an arbitrary path, pressure distribution, weight and shape. The circular path was only used as an example.

We also took a new approach to solve the circular case using the Hankel transform represented as the system of ordinary differential equations (5.12, 5.13). These sets were then solvable in the same way as in chapter 3 by using the Laplace transform. And though the numerical solution was not in complete agreement with the amplitude, we found that the wavelength and the wave speed were. In addition, the amplitude seemed to converge further away from the origin. Here further work may be needed. Another

approach may be to look for other options for computing the Hankel transform, by for example a quadrature solver.

Further work should be to investigate the 2D influence of a load moving over a surface using real-world experiments. Such experiments could help to verify accuracy of our model, and showing that the model is also usable not only in the special case of linear velocity. And if this is not the case then it could be possible to try out a more complicated model or try to include more of the non-linearities in (2.10, 2.6).

The appendix also contains a short paper written in collaboration with my supervisor Henrik Kalisch and Emilian Părău, based on the results from the model. To be submitted shortly.

Bibliography

[1] George D Ashton. *River and lake ice engineering*. Water Resources Publication, 1986.

[2] Natalie Baddour. Two-dimensional fourier transforms in polar coordinates. In *Advances in Imaging and Electron Physics*, volume 165, pages 1–45. Elsevier, 2011.

[3] Elliott Ward Cheney. *Analysis for applied mathematics*, volume 208. Springer, 2001.

[4] Walter Craig and Catherine Sulem. Numerical simulation of gravity waves. *Journal of Computational Physics*, 108(1):73–83, 1993.

[5] Evgueni Dinvay, Henrik Kalisch, and EI Părău. Fully dispersive models for moving loads on ice sheets. *Journal of Fluid Mechanics*, 876:122–149, 2019.

[6] Gerald B Folland. *Fourier analysis and its applications*, volume 4. American Mathematical Soc., 2009.

[7] AJS Hamilton. Uncorrelated modes of the non-linear power spectrum. *Monthly Notices of the Royal Astronomical Society*, 312(2):257–284, 2000.

[8] Don Hayley and Sam Proskin. Managing the safety of ice covers used for transportation in an environment of climate warming. In *4th Canadian Conference on Geohazards, Laval University, Quebec*, pages 20–24. Citeseer, 2008.

[9] Alexander Korobkin, Emilian I Părău, and Jean-Marc Vanden-Broeck. The mathematical challenges and modelling of hydroelasticity, 2011.

[10] Pijush K Kundu, Ira M Cohen, and David R Dowling. *Fluid mechanics*. Academic press, 2015.

[11] J Miles and Alfred D Sneyd. The response of a floating ice sheet to an accelerating line load. *Journal of Fluid Mechanics*, 497:435–439, 2003.

[12] F Milinazzo, Marvin Shinbrot, and NW Evans. A mathematical analysis of the steady response of floating ice to the uniform motion of a rectangular load. *Journal of Fluid Mechanics*, 287:173–197, 1995.

[13] David P Nicholls and Fernando Reitich. A new approach to analyticity of dirichlet-neumann operators. *Proceedings of the Royal Society of Edinburgh Section A: Mathematics*, 131(6):1411–1433, 2001.

[14] Alexander D Poularikas. *Transforms and applications handbook*. CRC press, 2018.

[15] Madeline Island Wilderness Preserve. Why is the ice road speed limit 15 mph?, 2018.
URL: `https://www.miwp.org/latest-news/2018/2/11/why-is-the-ice-road-speed-limit-15mph`.

[16] Rowan Romeyn, Alfred Hanssen, Bent Ole Ruud, and Tor Arne Johansen. Elastic properties of floating sea ice from air-coupled flexural waves. *The Cryosphere Discussions*, 2021:1–25, 2021.

[17] Konstantin Shishmarev, Tatyana Khabakhpasheva, and Alexander Korobkin. The response of ice cover to a load moving along a frozen channel. *Applied Ocean Research*, 59:313–326, 2016.

[18] Vernon Squire, Roger J Hosking, Arnold D Kerr, and Pat Langhorne. *Moving loads on ice plates*, volume 45. Springer Science & Business Media, 1996.

[19] Vernon A Squire. Ocean wave interactions with sea ice: A reappraisal. *Annual Review of Fluid Mechanics*, 52:37–60, 2020.

[20] Takatoshi Takizawa. Field studies on response of a floating sea ice sheet to a steadily moving load. *Contributions from the Institute of Low Temperature Science*, 36:31–76, 1988.

[21] Takatoshi Takizawa. Response of a floating sea ice sheet to a steadily moving load. *Journal of Geophysical Research: Oceans*, 93(C5):5100–5112, 1988.

[22] James D Talman. Numerical fourier and bessel transforms in logarithmic variables. *Journal of computational physics*, 29(1):35–48, 1978.

Ship Wave Patterns on Floating Ice Sheets

Kristoffer Johnson[1], Henrik Kalisch[1,*], and Emilian I. Părău[2]

[1]Department of Mathematics, University of Bergen, Postbox 7800, 5020 Bergen, Norway
[2]School of Mathematics, University of East Anglia, Norwich Research Park, Norwich, NR4 7TJ, UK
[*]henrik.kalisch@uib.no

ABSTRACT

This paper aims to explore the response of a floating icesheet to a load moving in a curved path. We investigate the effect of turning on the wave patterns and strain distribution, and exploring scenarios where turning increases the wave amplitude and strain in the ice, possibly leading to crack formation, fracturing and eventual ice failure. The mathematical model used here is the linearized system of differential equations introduced in[1], and the linear strain theory. The equations are solved using the Fourier transform in space, and the Laplace transform in time. The model is tested on known results for comparison, and several for compound trajectories involving turning and deaccelerating are tested.

Introduction

Hydro-elastic waves occur naturally in ice sheets in the arctic regions and on frozen lakes and sounds in the winter season. The study of such waves has a long history going back to the 1950's and was prompted by attempts to use solid ice covers as a means of supporting mechanized transportation. It was also recently shown[2,3] that such wave patterns can be observed using satellite synthetic-aperture radar (SAR) imagery.

In cold regions today, some winter truck routes are partially over ice-covered lakes, as this routing provides a low-cost alternative to building asphalt roads running along the lakeshores[4]. In some cases, these ice roads are the only economical means of transportation to reach remote communities in the North. These routes are also of major importance for mining operations in remote northern locations which depend on high-volume low-cost shipping of tools, equipment and lore.

Authorities in the northern regions follow various plans for opening and closing roads, maintaining safety by checking ice thickness, temperature and consistency, weather conditions, and planning routes based on local conditions and operational experience. In addition, an important component of ice road safety is proper instruction of truck operators. Maximal permitted loading is in many cases based on Gold's formula which relates the thickness of the ice cover to the allowable load based largely on empirical observations of ice failure or non-failure under various loading conditions[5].

In the case of heavy moving loads, the speed of the load is also an important factor in maintaining safety of ice roads. Indeed, it is well known that large speeds can create resonant waves in the ice cover and under certain conditions of speed, ice thickness, and water depth, the deflection under a vehicle travelling on a floating ice sheet may be amplified considerably. Under operational conditions, a speed limit of 15 mph (24 km/h) is often imposed. Exceeding the speed limit may lead to crack formation, and especially near the shore to so-called blowouts. Blowouts are usually caused by pressure build up due to waves reflecting off the shore, and interfering constructively with resonant waves excited by a heavy moving vehicle. Once a blow-out hole has formed, subsequent traffic must be rerouted.

While many early studies involving moving loads relied on constant load speed[6], the importance of incorporating transients was already highlighted in[7,8]. Non-constant load speeds are included in a few studies[1,9–12], and in particular it was shown numerically that a decelerating load could lead to constructive interference of waves which could exceed the critical stress and thereby lead to crack formation[1,12]. While some studies examine non-homogeneous ice conditions[13,14] and damping properties of the ice cover[15–20] which can be a major factor in ice failure, the present study is focussed on the effect of changes in speed and in particular changes in the direction of the moving load.

In the existing literature on theoretical modeling of hydroelastic waves induced by a moving load the focus has been exclusively on loads moving in a *straight path*. In the present contribution, we investigate the effect of a *curved path* on the waves created by the moving load. As already intimated above, curved vehicle trajectories are of interest because turning may sometimes be unavoidable due to routing problems, obstacles on the ice or localized ice failures. In addition, inexperienced drivers may be more likely to make sharp turns and velocity changes. As will be shown in the body of this article, curved paths may also lead to constructive interference which may be more dangerous than slowing down.

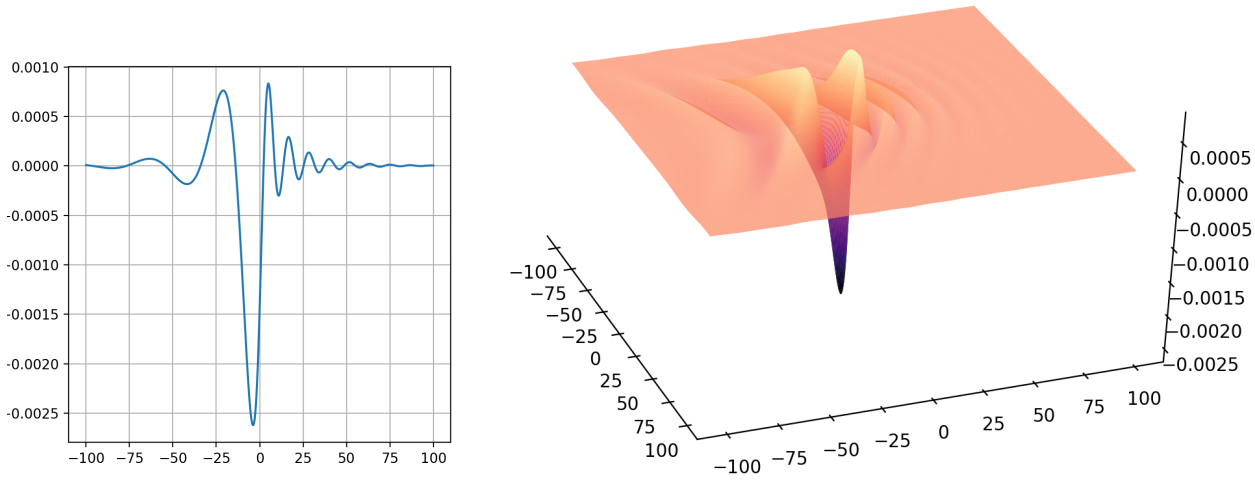

Figure 1. The left panel shows the central line of the right-hand plot the load is positioned at (x,y) = (0,0) and is travelling at 7 m/s the critical speed is 6 m/s. Axis units are in meters.

1 Mathematical model for hydro-elastic waves

We consider an inviscid, incompressible fluid of density ρ and undisturbed depth H, covered by a thin elastic solid of density ρ_I described by the Kirchhoff–Love plate theory (cf.[21]). For the purpose of describing hydro-elastic waves, one may assume irrotational flow, so that the flow in the fluid foundation is described by a potential $\phi(x,y,z,t)$ satisfying Laplace's equation $\triangle\phi = 0$. We assume that the thickness h of the elastic solid is small compared to both the depth and a typical wavelength. This simplification allows us to use a common coordinate system for the fluid and solid, and we specify that the fluid-solid interface is located at $z = \eta(x,y,t)$. At the interface, the trace of the velocity potential is defined by $\Psi(x,y,t) = \phi(x,y,\eta(x,y,t),t)$.

Using Hooke's law together with the second Kirchhoff hypothesis (i.e. assuming that normal stresses to surfaces parallel to the center surface are smaller than other stresses), the boundary condition at the solid-fluid interface can be written in terms of the hydroelastic parameter κ as a viscoelastic Bernoulli equation in the form

$$\kappa g\triangle^2\eta - \frac{\rho_I h^3}{12\rho}\partial_t^2\triangle\eta + \frac{\rho_I h}{\rho}\partial_t^2\eta + \frac{b}{\rho}\partial_t\eta + g\eta + \phi_t + \frac{1}{2}|\nabla\phi|^2 + \frac{P}{\rho} = 0. \tag{1}$$

In this equation, $\kappa = \frac{D}{\rho g}$ is the so-called hydro-elastic parameter, g denotes the gravitational acceleration, b is a damping coefficient and $P(x,y,t)$ denotes the imposed pressure due to the load. The second term in equation (1) takes account of horizontal acceleration in the solid. This effect is often neglected in the study of hydro-elastic waves, but in the present work this term is kept in the equation as it allows improved handling of the pressure forcing.

In virtually all cases where the ice can safely support a load, the deflection of the ice sheet is on the order of a a few millimetres which is small compared to all other length scales in the problem. As a result, it is generally a good approximation to consider the linear wave dynamics given by the linearized form of the equations. A particularly useful version of the equations is written in terms of the so-called Dirichlet Neumann operator G_0 relating Dirichlet to Neumann boundary data for the potential in the fluid foundation[22,23]. In terms of the interface deflection $\eta(x,y,t)$ and the trace of the potential $\Phi(x,y,t)$, the equations are written in the form

$$\eta_t = G_0\Phi, \tag{2}$$

$$\Phi_t = -g\frac{1+\kappa\triangle^2}{K}\eta - \frac{b}{\rho}\frac{G_0}{K}\Phi - w, \tag{3}$$

with the pressure forcing given in terms of $w = \frac{K^{-1}}{\rho}P(x,y,t)$. The equations are derived in[1] based on the approach used in[24,25]. The first equation is a linearized version of the kinematic boundary condition. The operator $1/K$ is defined as the inverse of

$$K = 1 + \frac{\rho_I h}{\rho}\left(1 - \frac{h^2\triangle}{12}\right)G_0. \tag{4}$$

It is shown in the Appendix, how the operators K and G_0 can be written more explicitly using the two-dimensional Fourier transform. The system of equations (2)-(3) accurately describes the dynamics of a wave of arbitrary wavelength, and is therefore known as a fully dispersive system[24,26].

The system can be solved using the Laplace transform $\mathscr{L}$. Indeed, defining the operators

$$R = \frac{bG_0}{2\rho K} \quad \text{and} \quad U = \sqrt{\frac{g(1+\chi\partial_x^4)G_0}{K} - R^2},$$

then for zero initial data, the solution takes the form $\eta = \mathscr{L}^{-1}(\hat{m}(s)\cdot\hat{w}(s))$, where $\hat{m}$ denotes the Laplace transform of $m = \mathscr{L}^{-1}((\frac{-G_0}{(s+R)^2+U^2})$ and $\hat{w}$ denotes the Laplace transform of $w = \frac{K^{-1}}{\rho}\cdot P(x,y,t)$.

As is customary, an expression for $\eta(x,y,t)$, can be found use the convolution identity

$$\mathscr{L}^{-1}(\hat{m}(s)\cdot\hat{w}(s)) = \mathscr{L}^{-1}(\hat{m}(s)) * \mathscr{L}^{-1}(\hat{w}(s)) = m * w, \tag{5}$$

defined explicitly as

$$\eta(\cdot,t) = \int_0^t m(t-\tau)w(\tau)d\tau.$$

The integral kernel m is given by the inverse Laplace transform $\mathscr{L}^{-1}(\hat{m}(s))$ which can be solved exactly in the form

$$\mathscr{L}^{-1}(\hat{m}(s))(t) = \frac{G_0}{2iU}\left(e^{-(t-\tau)(R-iU)} - e^{-(t-\tau)(R+iU)}\right). \tag{6}$$

In some works, the load is assumed to be rectangular, but due to the inclusion of rotary inertia and the scale separation between the load and the wavelength of the excited waves, one my also consider a point load. In the present case, since the load is following a curved path, it is most expedient to use either a point load, or a symmetric Gaussian distribution which will be rotation-invariant under the change in orientation during the turns. Assuming for the moment that the load is given by a point mass w_0, and is following a path parametrized by the vector $\vec{X}(t) = [x(t), y(t)]$, then the time evolution of the load position is given in terms of the Fourier transform as $w(\cdot,t) = w_0 e^{i\vec{X}(t)\cdot\vec{\xi}}$. It then transpires that the deflection has the form

$$\int_0^t m(t-\tau)w_0 e^{i\vec{X}(t)\cdot\vec{\xi}}d\tau, \tag{7}$$

where $\vec{\xi} = (\xi_1, \xi_2)$ is a vector in Fourier or wavenumber space. Since we have the Fourier multiplier operator $m(t)$ in explicit form, we can find the general solution as an integral as

$$\int_0^t \frac{G_0 w_0}{2iU}\left(e^{-(t-\tau)(R-iU)} - e^{-(t-\tau)(R+iU)}\right)e^{i\vec{X}(\tau)\cdot\vec{\xi}}d\tau. \tag{8}$$

Strictly speaking the term $e^{i\vec{X}(\tau)\cdot\vec{\xi}}$ should be written as $\mathscr{F}^{-1}e^{i\vec{X}(\tau)\cdot\xi}\mathscr{F}$, but we have used a shorthand notation for easier reading. For reasons that will be apparent later it is convenient to keep the solution as two separate integrals, but for compactness and because it looks tidier, we mention that some simplifications get us to the form

$$\eta(x,t) = \frac{G_0 w_0}{U}\int_0^t e^{-(t-\tau)R}e^{-i\vec{X}(\tau)\cdot\vec{\xi}}\sin[(\tau-t)U]\,d\tau. \tag{9}$$

This integral can be solved analytically in some cases, but in general it has to be evaluated numerically. In the case of a Gaussian load distribution, the formulas above are slightly more involved, but the final solution may also be written in explicit form.

Given a solution $\eta(\cdot,t)$, the corresponding shear strain can be computed using linear strain theory as used for example in[27]. In order to obtain the maximum strain, one may use the maximum eigenvalues of the Hessian matrix $\sigma_{ij} = \partial_i\partial_j\eta\cdot\frac{h}{2}$ scaled by $h/2$ where we recall that h is the thickness of the ice sheet.

2 Numerical methods

In order to compute the deflection of the ice sheet due to a moving load, the various integrals given above need to be evaluated. In addition, since most spatial operators are given in terms of Fourier multipliers, the FFT and inverst FFT are used. In this discrete approximation, a finite set of N wavenumbers is used (in each dimension). In the case of the two-dimensional discrete Fourier transform, the wavenumber vector is the vector $\vec{k}(n) = [k_1(n), k_2(n)]$, where $n = [-N/2-1, N/2]$.

While it is possible to use a point load without any problem, the computations are more stable (in particular when approximating the strain) so all results here are given for a load with a circular Gaussian weight distribution. It also makes physical sense that the load be distributed over a finite area.

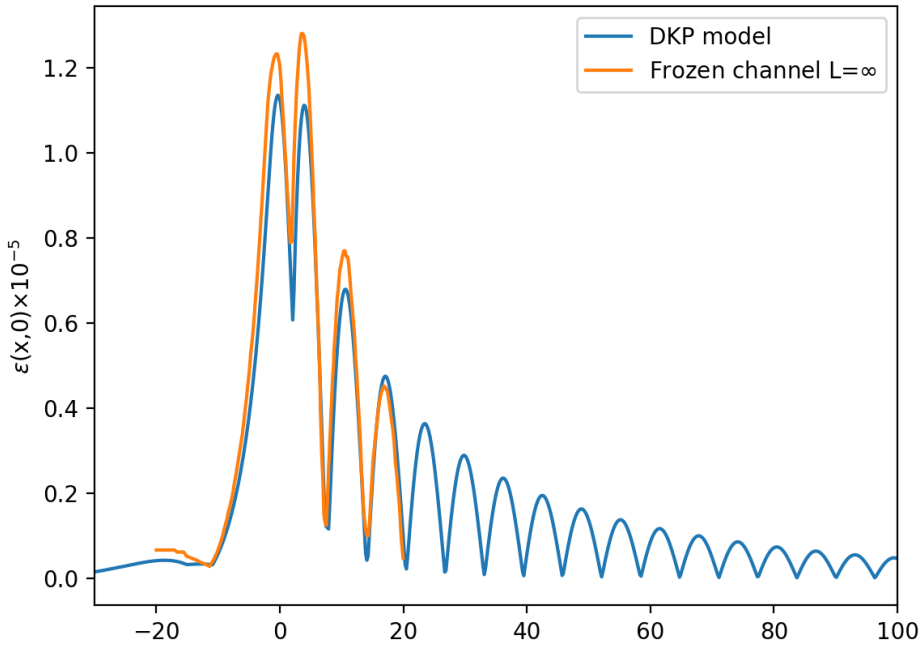

Figure 2. Strain due to wave excited by moving load. SKK Model[27] compared to DKP 3.

The integration procedure is as follows. For example, if we have a path with two parts, say a straight path followed by a turn parameterized by the functions $X(t) = X_1(t)$, for $0 \le t < c$ and $X_2(t)$, for $c < t < T$, then it may be convenient also to split the integral for the solution (8) into two parts. If we want a part of the first solution we only need to integrate over X_1 but if we afterwards want the solution on the second part of the path, we still have to evaluate the whole integral

$$\frac{G_0 w_0}{2iU}\left(\int_0^t (e^{-(t-\tau)(R-iU)} e^{i\vec{X}(\tau)\cdot\vec{\xi}} d\tau - \int_0^t e^{-(t-\tau)(R+iU)} e^{i\vec{X}(\tau)\cdot\vec{\xi}} d\tau\right). \tag{10}$$

If we now define the two integrals over $X_1(t)$ as

$$I_1 = \int_0^c (e^{-(t-\tau)(R-iU)} e^{i\vec{X}(\tau)\cdot\vec{\xi}} d\tau,\ I_2 = \int_0^c (e^{-(t-\tau)(R+iU)} e^{i\vec{X}(\tau)\cdot\vec{\xi}} d\tau, \tag{11}$$

then the final solution for $t > c$ can be written as

$$\frac{G_0 w_0}{2iU}\left(e^{-(t-c)(R-iU)} I_1 + \int_c^t e^{-(t-\tau)(R-iU)-i\vec{X(\tau)}\cdot\vec{\xi}} d\tau - e^{-(t-c)(R+iU)} I_2 - \int_c^t e^{-(t-\tau)(R+iU)-i\vec{X(\tau)}\cdot\vec{\xi}}\right). \tag{12}$$

Of course, depending on the situation, one may split the path at any point, and once could even define the solution at any time point using an iterative prosses of the discrete time steps. Another way to do this is to compute $\Phi(x,t)$ and use the previous

solution as initial conditions, and propagate the solution that way. An example of the integral method is in the first contour plots in the next section, where a straight path is followed by a circular one.

In order to test our solution strategy and the numerical implementation, we compare this with the strain shown in[27] where the response of an ice cover to a moving load is considered. In that work, the ice cover is fixed to vertical walls at the boundary, so that some deviation is to be expected. Nevertheless, comparing the results from the present study (shown in the left panel) to the response computed in[27] (shown in the right panel), one may conclude that the results line up quite well, at least for the central line $\varepsilon(x,0)$ shown in the right panel of Figure 2.

3 Results

3.1 Ship-wave patterns for circular paths

We illustrate the response to various paths taken by the moving load. In the examples shown below, we are looking at the case when the depth of the fluid base is $H = 6.8$m the thickness of the ice sheet is $h = 0.17$m, and the flexural rigidity is $\mathscr{D} = 2.35 \times 10^5$, so that the hydro-elastic parameter is $\kappa = 23.3\text{m}^4$, and the critical load speed is $v_c = 6.0$m/s, the same case as in[28,29].

First, we display the "ship wave pattern" excited by a load moving in a straight path (Figure 3a). Then we display how the pattern changes when part of the path is curved (Figure 3b). Finally in Figure 3c, we show the pattern excited by a path which moves in a straight path followed by a full circle. Due to the damping the waves excited during the straight part of the path are already too small to be visible in Figure 3c. Figure 4 shows a three-dimensional plot of the wave response to a moving load in a partial or full circle, corresponding to Figure 3b and Figure 3c.

Finally, Figure 5 shows the wave pattern after the vehicle continues moving in the same circle. In this case, due to the damping, a quasi-steady wave pattern emerges which appears to move outward in a spiral pattern. This type of behaviour may grant further investigation, in particular from a mathematical point of view. This is left for future work. However we now turn to the potential danger incumbent in making turns of varying radius.

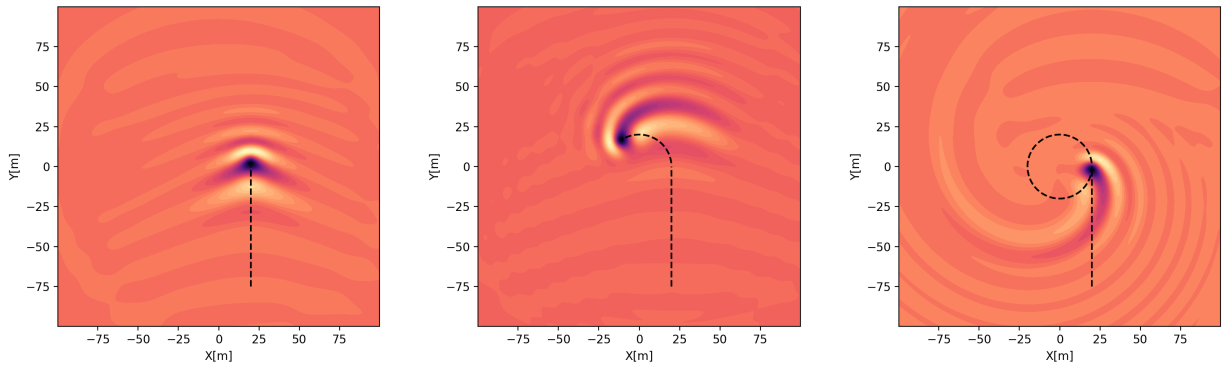

Figure 3. Wave pattern excited by a vehicle of weight 235kg on an ice plate of thickness $h = 0.17$m over a fluid foundation of depth $H = 6.8$m. Panel A shows the vehicle at the beginning before the turn has been started ($t = 0.32s$). Panel B shows the wave pattern while the vehicle is turning at $t = 6.5$s. Panel C shows the wave pattern after one full turn has been completed at $t = 19$s. Axis units are in meters.

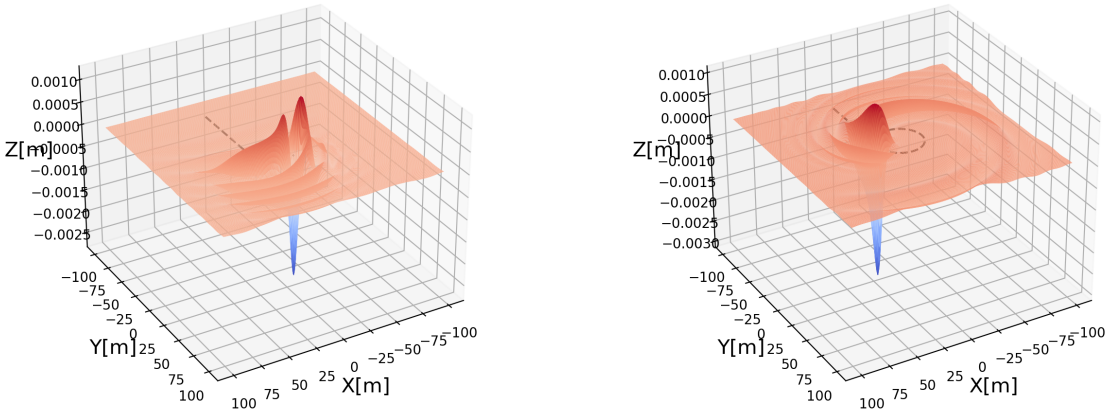

Figure 4. Left panel: Three-dimensional wave pattern at $t = 6.5$s. Right panel: Three-dimensional wave pattern at $t = 19$s. The parameters are the same as in Figure 3. Axis units are in meters.

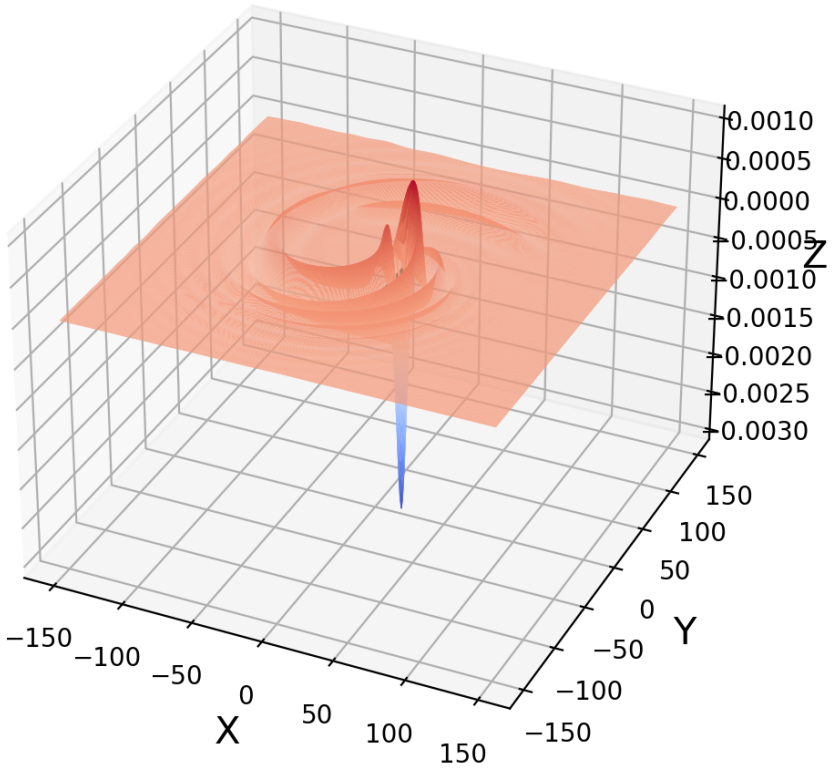

Figure 5. A three-dimensional plot of the wave response at $t = 38.7$s. Note that a quasi-steady wave pattern emerges as the vehicle continues to go in a circle. The parameters are the same as in Figure 3. Axis units are in meters.

3.2 Turning on an ice road

As mentioned in the introduction, ice roads are a vital part of the infrastructure in cold regions such as Canada, supporting remote communities and mining operations[4]. Popularized by epic TV productions such as *Ice Road Truckers*, ice roads have also become somewhat of a tourist attraction[30]. In the age of global warming, ice thickness variations have become more unpredictable, and the managing and maintenance of ice roads has become more difficult[4]. If many inexperienced drivers such as tourists use the ice roads, it can have an impact on the overall safety of the roads. All ice roads require strict speed limits which range from 4mph (6.5km/h) on very shallow lakes to 15mph (24km/h) on most roads and up to 22mph (35 km/h) on deep lakes[31]. It is well known that if a vehicle exceeds the critical speed for a particular configuration depending on the depth of the fluid foundation, the ice thickness and the ice consistency (e.g. salinity, temperature, enclosed impurities), resonances in the hydro-elastic system create waves propagating independently of the load. Especially in near-

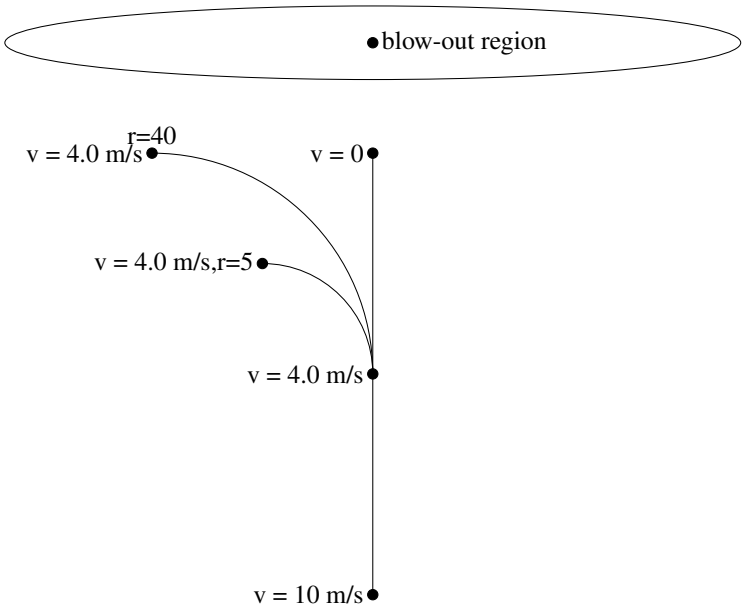

shore locations, these waves can create dangerous ice excursions as the waves may interact with the shoreline, and the reflections can interfer constructively with the still incoming waves. This may lead to so-called blowouts, often in the near-shore region. Due to blowouts and other obstacles, rerouting of traffic may become necessary. In what follows, we examine the safety of turning on the ice.

We look at an idealized case where a vehicle travels at a relatively high speed of 36km/h ($\sim$ 10m/s) a speed that might be considered safe on a deep lake. If the vehicle enters a shallower area either nearshore or due to a shoal in the lake, it might be in a position where the critical speed is much lower. If there is a blow-out region or an obstacle in front, the vehicle will either have to slow down or turn in order to avoid the obstacle. Say that at 4m/s = 14.4km/h the driver contemplates turning. Because of the decreasing depth, the critical speed is now only 3.13m/s = 11.3km/h, so the vehicle travels at supercritical speed. For the sake of being explicit, we look at the case of a 1000kg vehicle on an ice cover of thickness $h = 0.2$m. This would correspond to using Gold's formula with a rather conservative choice of the constant $A = 2.5$ from the golds formula defining the likelihood of ice failure[5].

From the plots shown in Figure 6, the most dangerous action seems to be turning too early with a large radius (red and green curves). This path puts a lot more stress on the ice over and for a greater time. For the 5-meter turning radius, the strain in the model actually decreases, but as traction will always be a problem when driving on ice a turn with a 5-meter radius might be unfeasible. Therefore, even if aiming for a sharp turn, the driver might end up in a turn with a larger radius adding a potentially uncontrolled vehicle to the mix. The safest behaviour in this case would to try to stop in front of the blow-out, though this may not be possible either.

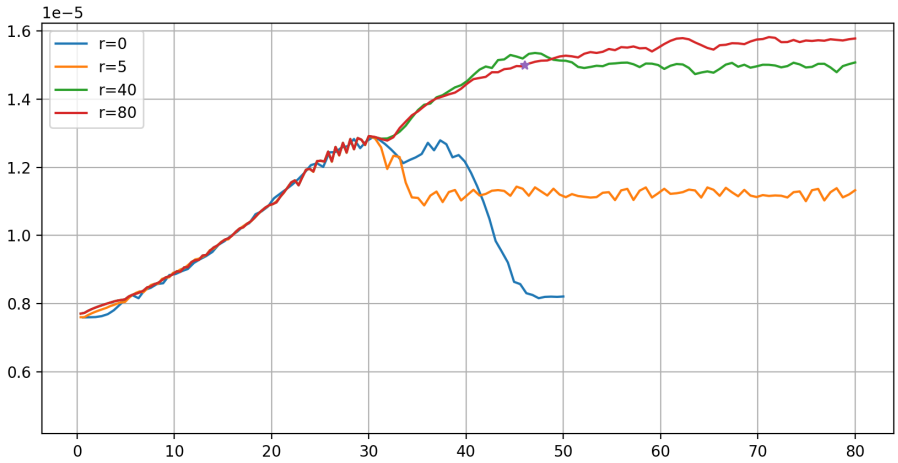

Figure 6. Maximal strain vs. time due to wave response to a vehicle of weight 1000kg on an ice sheet of thickness $h = 0.2$m over a fluid foundation of depth $H = 1$m. Blue curve: slowing down, no turn, continue at slower speed. Yellow curve slowing down at same rate as blue curve, turning at slower speed, radius of turn is $r = 5$m. Green curve slowing down at same rate as blue curve, turning at slower speed, radius of turn is $r = 40$m. Red curve slowing down at same rate as blue curve, turning at slower speed, radius of turn is $r = 80$m.

4 Conclusions

The subject of this paper has been to study a mathematical model which enables the efficient description of wave patterns induced by loads moving on ice sheets in curved paths. It was shown how the model (2)-(3) can be solved explicitly for a load traveling in a curved path. While the present work concentrated on point loads and Gaussian distributed loads, any other foorprint and weight distribution of load can be handled. Loads moving in a straight path and in a circular path have been considered, but the method laid out here applies to an arbitrary curved load path.

It is well known that on ice roads, speed related blowouts may occur. Ice roads are particularly treacherous near the shore, as the critical speed is smaller due to smaller depth, and wave reflecting off the shore may combine with waves generated by a moving vehicle to crack the ice. Even for expert operators, keeping below the critical speed may be difficult at times, as the most important factor is the depth of the water beneath the ice. If conditions are right the critical speed can drop as low as 10km/h[4], and slowing down followed by turning may in some cases be dangerous even in conditions which would be otherwise considered safe. Indeed it has been shown that changes in direction can have a sginificant effect on the strain in the ice induced by the waves excited by the moving load.

A Fourier multiplier operators

For the convenience of the reader, we recall the definition of various Fourier multiplier operators. The operators G_0 and K are defined in terms of the (two-dimensional) Laplacian $\triangle_H = \partial_x^2 + \partial_y^2$ as

$$G_0 = \sqrt{\triangle}\tanh(H\sqrt{\triangle}),$$

$$K = 1 + \frac{\rho_I h}{\rho}\left(1 - \frac{h^2\triangle}{12}\right)G_0.$$

These operators can be written in terms of the Fourier transform

$$\hat{f}(\xi_1,\xi_2) = \mathscr{F}\{f(x,y)\} = \int_{-\infty}^{\infty} f(x,y)e^{-i\xi_1 x - i\xi_2 y}\,\mathrm{d}x\mathrm{d}y, \tag{13a}$$

and the inverse Fourier transform

$$f(x,y) = \mathscr{F}^{-1}\{\hat{f}(\xi_1,\xi_2)\} = \frac{1}{2\pi}\int_{-\infty}^{\infty} \hat{f}(\xi_1,\xi_2)e^{i\xi_1 x + i\xi_2 y}\,\mathrm{d}\xi_1\mathrm{d}\xi_2. \tag{13b}$$

We have

$$G_0 = \mathscr{F}^{-1}\left\{\sqrt{\xi_1^2+\xi_2^2}\,\tanh\left(H\sqrt{\xi_1^2+\xi_2^2}\right)\right\}, \tag{14}$$

so that $G_0 f = \mathscr{F}^{-1}\left\{\sqrt{\xi_1^2+\xi_2^2}\,\tanh\left(H\sqrt{\xi_1^2+\xi_2^2}\right)\right\}\mathscr{F}f$. Similarly, we have

$$K = \mathscr{F}^{-1}\left\{1 + \frac{\rho_I h}{\rho}(1 + \frac{h^2}{12}(\xi_1^2+\xi_2^2))\sqrt{(\xi_1^2+\xi_2^2)} * \tanh\left(H\sqrt{(\xi_1^2+\xi_2^2)}\right)\right\}. \tag{15}$$

References

1. Dinvay, E., Kalisch, H. & Părău, E. Fully dispersive models for moving loads on ice sheets. *J. Fluid Mech.* **876**, 122–149 (2019).
2. Babaei, H., Van der Sanden, J., Short, N. & Barrette, P. Lake ice cover deflection induced by moving vehicles: comparing theoretical results with satellite observations. In *New Research and Developments in Road Safety Session of the 2016 Conference of the Transportation Association of Canada Toronto, ON* (2016).
3. Van der Sanden, J. & Short, N. Radar satellites measure ice cover displacements induced by moving vehicles. *Cold Reg. Sci. Technol.* **133**, 56–62 (2017).
4. Hayley, D. & Proskin, S. Managing the safety of ice covers used for transportation in an environment of climate warming. In *4th Canadian Conference on Geohazards, Laval University, Quebec*, 20–24 (Citeseer, 2008).
5. Gold, L. W. Use of ice covers for transportation. *Can. Geotech. J.* **8**, 170–181 (1971).
6. Davys, J., Hosking, R. & Sneyd, A. Waves due to a steadily moving source on a floating ice plate. *J. Fluid Mech.* **158**, 269–287 (1985).
7. Kheysin, D. Y. & Yakovlev, G. Some unsteady-state problems in ice-cover dynamics. *Stud. ice physics ice engineering (ed. GN Yakovlev)* 69–78 (1973).
8. Schulkes, R. M. S. M. & Sneyd, A. D. Time-dependent response of floating ice to a steadily moving load. *J. Fluid Mech.* **186**, 25–46 (1988).
9. Miles, J. & Sneyd, A. D. The response of a floating ice sheet to an accelerating line load. *J. Fluid Mech.* **497**, 435–439 (2003).
10. Pogorelova, A. Wave resistance of an air-cushion vehicle in unsteady motion over an ice sheet. *J. applied mechanics technical physics* **49**, 71–79 (2008).
11. Sturova, I. V. Unsteady three-dimensional sources in deep water with an elastic cover and their applications. *J. Fluid Mech.* **730**, 392–418 (2013).
12. Hosking, R. J. & Milinazzo, F. Two-dimensional response of a floating ice plate to a line load moving at variable speed. *J. Fluid Mech.* **938** (2022).

13. Romeyn, R., Hanssen, A., Ruud, B. O. & Johansen, T. A. Elastic properties of floating sea ice from air-coupled flexural waves. *The Cryosphere Discuss.* **2021**, 1–25 (2021).

14. Sturova, I. Motion of a load over an ice sheet with non-uniform compression. *Fluid Dyn.* **56**, 503–512 (2021).

15. Hosking, R., Sneyd, A. D. & Waugh, D. Viscoelastic response of a floating ice plate to a steadily moving load. *J. Fluid Mech.* **196**, 409–430 (1988).

16. Zhestkaya, V. Numerical solution of the problem of an ice sheet under a moving load. *J. applied mechanics technical physics* **40**, 770–775 (1999).

17. Wang, K., Hosking, R. & Milinazzo, F. Time-dependent response of a floating viscoelastic plate to an impulsively started moving load. *J. Fluid Mech.* **521**, 295–317 (2004).

18. Kozin, V. & Pogorelova, A. Effect of the viscosity properties of ice on the deflection of an ice sheet subjected to a moving load. *J. Appl. Mech. Tech. Phys.* **50**, 484–492 (2009).

19. Marchenko, A. & Cole, D. Three physical mechanisms of wave energy dissipation in solid ice. In *Proceedings of the International Conference on Port and Ocean Engineering Under Arctic Conditions* (2017).

20. Dinvay, E., Kalisch, H. & Părău, E. Waves generated by moving loads on ice plates: viscoelastic approximations. *submitted* (2022).

21. Squire, V., Hosking, R. J., Kerr, A. D. & Langhorne, P. *Moving loads on ice plates*, vol. 45 (Springer Science & Business Media, 1996).

22. Craig, W., Guyenne, P. & Kalisch, H. Hamiltonian long-wave expansions for free surfaces and interfaces. *Commun. on Pure Appl. Math.* **58**, 1587–1641 (2005).

23. Craig, W. & Sulem, C. Numerical simulation of gravity waves. *J. Comput. Phys.* **108**, 73–83 (1993).

24. Moldabayev, D., Kalisch, H. & Dutykh, D. The whitham equation as a model for surface water waves. *Phys. D: Nonlinear Phenom.* **309**, 99–107 (2015).

25. Dinvay, E., Kalisch, H., Moldabayev, D. & Părău, E. I. The Whitham equation for hydroelastic waves. *Appl. Ocean. Res.* **89**, 202–210 (2019).

26. Aceves-Sánchez, P., Minzoni, A. & Panayotaros, P. Numerical study of a nonlocal model for water-waves with variable depth. *Wave Motion* **50**, 80–93 (2013).

27. Shishmarev, K., Khabakhpasheva, T. & Korobkin, A. The response of ice cover to a load moving along a frozen channel. *Appl. Ocean. Res.* **59**, 313–326 (2016).

28. Takizawa, T. Field studies on response of a floating sea ice sheet to a steadily moving load. *Contributions from Inst. Low Temp. Sci.* **36**, 31–76 (1988).

29. Takizawa, T. Response of a floating sea ice sheet to a steadily moving load. *J. Geophys. Res. Ocean.* **93**, 5100–5112 (1988).

30. The North's Cool Highways *Nortwest Territories Tourism*, Spectacular Northwest Territories https://spectacularnwt.com/ (2021).

31. Why Is the Ice Road Speed Limit 15 mph? *Madeline Island Wilderness Preserve*, Spectacular Northwest Territories url = https://www.miwp.org/latest-news/2018/2/11/why-is-the-ice-road-speed-limit-15mph, (2018).

Appendix A

Code used in the experiments

Underneath is a few examples of codes used to compute critical speed, the general operators and the circular path:

Listing A.1: Computing Critical Speed

```
def CS(H,L, g = 9.81,uc = True):
    """ The critical speed given by the H and L """
    HL = H/L

    def F(X):
        return ((3 +
            ↪ (2*HL/X)/np.sinh(2*HL/X))/(1-(2*HL/X)/np.sinh(2*HL/X)))**(1/4)
            ↪ - X

    X_c = newton(F,0.1)

    U_c = np.sqrt((X_c + 1/X_c**3)*np.tanh(HL/X_c))

    if uc == False:
        return U_c
    u_c = U_c*np.sqrt(g*L)


    return u_c
```

Listing A.2: Computing the common operators for use in the different cases

```
def GetOperators(l,m,fname = 'Gaussian',arg = 'gaus'):

    """ Parameters : l,m Returns dx,X,Y,ksi1,ksi2,Fhatk,G_0k,Fkk,Rk,Uk
        ↪ """

    variables = GetVariables()

    rho = variables['rho']
    b = variables['b']
    rho_i = variables['rho_i']
    h = variables['h']
    H = variables['H']
    g = variables['g']
    L = variables['L']

    if arg == 'gaus':
```

```
        gaus = variables['gaus'] # its understod that if nothing else is mentioned then we use the standard gaussian distriution
        arg = gaus

    dx = l*2/m

    #-------------fourier grid--------------
    freq = fft.fftfreq(m,dx/2/np.pi)

    ksi1,ksi2 = np.meshgrid(freq,freq)
    # the ksi of zero canot be equal to zero or else there wil be a divide by zero error

    ksi1[:,0] = 0.00001
    ksi2[0,:] = 0.00001

    #-----------fourier operators-------------

    rr = ksi1**2 + ksi2**2

    Fkk = 1 + rho_i*h/rho*(1+(h**2)*rr/12)*np.sqrt(rr)*np.tanh(H*np.sqrt(rr))

    G_0k = np.sqrt(rr)*np.tanh(H*np.sqrt(rr))

    Rk = b*G_0k/(2*rho*Fkk)

    Uk = np.sqrt(g*(1+L**4*(rr**2))*G_0k/Fkk - Rk**2)

    #------------------X,Y grid---------------

    u = np.linspace(-l,l,m)

    X,Y = np.meshgrid(u,u)

    if fname in initialFuncs:
        Fb = initialFuncs[fname]
    else:
        print(fname + " is not found in initial funcs" + "valid names are:" + str(initialFuncs.keys()))



    Fhatk = fft.fftn(Fb(X,Y,arg))
    Fhatk = Fhatk

    #---------------this is just the procedure of extracting all of the oppreators-----------------
    Liste = [dx,X,Y,ksi1,ksi2,Fhatk,G_0k,Fkk,Rk,Uk]

    names = ['dx','X','Y','ksi1','ksi2','Fhatk','G_0k','Fkk','Rk','Uk']

    operators = dict()

    for (name,item) in zip(names,Liste):
        operators[name] = item

    return operators
```

Listing A.3: Example circular path first version

```
def CPslowT(r,v,a,T,l,m):
    """ paramters : alpha_0,r,v,a,t,l,m , where a is the deacceleration \n
    returns integrals I_1 and I_2 \n
    a is only given in total deacceleration so no need for deviding by r
    """

    operators = GetOperators(l,m)
    variables = GetVariables()
    rho = variables['rho'],



    Uk = operators['Uk']
    Rk = operators['Rk']
    G_0k = operators['G_0k']
    Fhatk = operators['Fhatk']
    ksi1 = operators['ksi1']
    ksi2 = operators['ksi2']
    Fkk = operators['Fkk']
    dx = operators['dx']

    alpha = v/r

    a = a/r

    print(v)
    print(a)

    @jit(nopython=True)
    def X_1(tau):
        return  r*np.cos((alpha + 0.5*a*tau)*tau)

    @jit(nopython=True)
    def X_2(tau):
        return r*np.sin((alpha + 0.5*a*tau)*tau)

    t = T[-1]

    t_0 = T[0]
    I = []
    sum1 = np.zeros(np.shape(ksi1))
    sum2 = np.zeros(np.shape(ksi1))

    for t in T[1:]:

        front = G_0k*complex(0,1)*Fhatk/2/Uk/Fkk



        @jit(nopython=True)
        def i_1(tau):
            return front*np.exp((tau-t)*(Rk-complex(0,1)*Uk) - complex(0,1)*(X_1(tau)*ksi1 + X_2(tau)*ksi2))

        @jit(nopython=True)
        def i_2(tau):
            return front*np.exp((tau-t)*(Rk+complex(0,1)*Uk) - complex(0,1)*(X_1(tau)*ksi1 + X_2(tau)*ksi2))

        print(" staring integration i_1")
        tt = time.time()

        I_1,err1,info1 = quad_vec(i_1,t_0,t,full_output=True,epsrel = 1e-14,epsabs = 0, workers = 1)

```

```
63
64          print("starting integration i_2")
65          tt = time.time()
66
67          I_2,err2,info2 = quad_vec(i_2,t_0,t,full_output=True,epsrel =
                ↪ 1e-14,epsabs = 0,workers = 1)
68          print("Time =" + str( time.time()-tt) + "estimated error is:"
                ↪ + str(err2))
69
70          # Just the last part where it is scaled and translated into
                ↪ position
71
72          ii1 = np.exp(-(t-t_0)*(Rk - complex(0,1)*Uk))
73
74          ii2 = np.exp(-(t-t_0)*(Rk + complex(0,1)*Uk))
75
76
77
78          sum1 = sum1*ii1 + I_1
79          sum2 = sum2*ii2 + I_2
80
81          t_0 = t
82
83          I.append([sum1,sum2])
84
85      return I
```

A.3 is an install version that only utilizes the the GetOperators and the GetVariables command. If this one is copied and used in conjunction with the program GetOperators() A.2 and the the variables are filled in stead of using the GetVariables one should be able to replicate the results. The initial function is needed in A.2 and can be hardcoded in as F = ... In the original program a separate enviroment was used to store initial functions.A.1 is used to compute the critical speed, and is only needed to get the speed ranges for where interesting stuff starts to happen as described in chapter 2. Example of what the critical speed is is shown in 2.2.

And ksi1, ksi2 is set to be above 0 as otherwise Uk would be zero and one would be dividing by zero later on in the solution.